INTRACELLULAR LABELING OF LIVE CELLS VIA TRANSIENT MEMBRANE PERMEABILIZATION FOR FLUORESCENCE AND SUPER RESOLUTION MICROSCOPY

BY

KAI WEN TENG

DISSERTATION

Submitted in partial fulfillment of the requirements
for the degree of Doctor of Philosophy in Biophysics and Computational Biology
in the Graduate College of the
University of Illinois at Urbana-Champaign, 2016

Urbana, Illinois

Doctoral Committee:

Professor Paul R. Selvin, Chair
Professor Steven C. Zimmerman
Associate Professor Charles M. Schroeder
Assistant Professor Kai Zhang

Abstract

Fluorescence imaging of intracellular proteins is often achieved by using transfection-induced expression of fluorescent protein. This can potentially impose artifacts such as loss of function or over-expression of target proteins. Direct labeling of the intracellular protein is an alternative to transfection, but is largely limited by permeability of the fluorescent probes. Here, we have developed a high-throughput technique for labeling intracellular proteins of living cells. The technique makes use of Streptolysin O (SLO), a bacterial enzyme that permeabilizes cells to DNA, RNA, proteins. We show that SLO can be used to deliver a variety of fluorescent probes; ranging from organic dyes (<1 kDa in size) to fluorescent immunoglobulin antibody (~150 kDa) for specific labeling of intracellular proteins. We demonstrate in numerous ways that after permeabilization the cells remained viable and responded normally to cell signaling protein. We applied this technique to observe the dynamic motion of labeled actin and mitochondria using super-resolution fluorescence microscopy (dSTORM). Furthermore, we show the ability to image single proteins inside the living cell by tracking single molecules of kinesin using photostable probes.

Acknowledgements

I am very fortunate to have met many great scientists and people throughout my doctorate study, without them the completion of this doctorate study would not be possible. I want to thank my advisor Paul Selvin for his guidance, support, and encouragements. Paul offered me an opportunity to work in his lab when I was very confused about my path forward, which I will be forever grateful. I am also very appreciative for the advices I received from our experienced and knowledgeable post-docs, Sang Hak Lee, and Yuji Ishitsuka. They spent a lot of time offering advices on my projects. I am thankful for the helps and companionship I received from current and past Selvin Lab members, especially Marco Tjioe, Duncan Nall, Janet Sheung, Chaoyi Jin, Pin Ren, Pinghua Ge and Yeoan Youn. Because of them it was always enjoyable to go to work and spend time in the lab. I want to thank visiting scholar Andre De Thomaz for all the lunch companionship and words of encouragement. I also want to thank Tobias Rosenkranz and his wife Pallu T. Rosenkranz for teaching me protein purification and sold me my first car.

The first half of my doctorate study was spent in Professor Bob Clegg's lab, who unfortunately passed away during the 4th year of my doctorate study. Bob taught me to be creative in research, and made me appreciate the very fundamental aspects of science, which I will always remember. I especially want to thank my mentor John Eichorst, who was a remarkable scientist and friend. He taught me about dedication and self-motivation, which I now appreciate very much. I also want to thank other former lab member of Clegg Lab, Ulai Noomnarm and David Park, whom I continued to be friend with even after the disband of the Clegg lab.

I want to thank my parents and my family for allowing me to pursuit my doctorate study for so many years. I am sorry for all the times that I am not there with them. I want to thank my

wife Wendy, who made the past 12 years of my life in Binghamton and Champaign the best time of my life.

Throughout my doctorate study I've almost always been supported by teaching assistantship. I appreciate the occasional change of theme from research to teaching. So therefore I want to thank all the students I've taught so far. They were great students, and I had a great time teaching and interacting with them.

I want to thank the Physics and Biophysics departments, especially the personnel and secretaries, who resolved many problems for us and processed our paperwork very patiently.

I also want to acknowledge L.S. Edelheit Fellowship for support that I received. I am especially appreciative of this award, because this is the first ever award I received for performing research.

Lastly, I want to thank my previous and last-minute appointed thesis committee members, who had agreed to be on my thesis committee without being on my prelim committee due to special circumstances. I understand that my requests were very last minute, and I appreciate them being able to attend the thesis defense.

Table of Contents

Chapter 1

Introduction and Background

1.1 LABELING INTRACELLULAR PROTEINS OF LIVING CELLS

The eventual goal of many biophysical experiments is to be able to observe how a particular protein functions in the dynamic system of a living cell. Fluorescence and super-resolution fluorescence microscopy provide us with the tools to do just that; it became possible to visualize a particular protein over the background. To achieve this, many experimental designs has included the use of transfected cell, where a green fluorescent protein (GFP), or any fluorescent proteins (FP) are appended to the protein of interest. The consideration for attaching a FP is always this; how much does adding a GFP affect the function of the target protein. Most importantly, the over-expression of target protein from transfection can cause serious artifact in the biological results that one obtains. What we really want is a way to introduce fluorescent probes, which targets a specific protein, inside a living cell. This is a significant challenge, because unlike using cells that are fixed and permeabilized, the cell membrane of a healthy cell is not permeable to most of the fluorescent probes. There are two ways to tackle this problem; from the designing of probe itself, or find some ways to bypass the membrane either mechanically or chemically. In terms of probe design, various combinations of cell permeant fluorophore and ligands have been use to get by the cell membrane. For example, small cell permeant ligands that are able to form covalent bond with protein of interest that carries specific tags has become increasingly popular; namely, chloroalkane (for HaloTag)[1], benzylguanine (for SNAPtag)[2], and trimethoprim-Acrylamide (for eDHFR)[3]. In order to label protein of interest using these novel labeling system, the cells has to first be transfected with either Halotag enzyme, SNAPtag enzyme or eDHFR fused to the protein of interest. To retain the permeability

of the fluorescent probe, the ligand has to be conjugated to a cell permeant dye. Some examples of these cell permeant organic dyes are Oregon Green, tetramethylrhodamine (TMR), silicon Rhodamines (siR) and Atto655. The fluorescent probes would label intracellular proteins when incubated with the cell, and excessive probes are usually washed away by incubating with serum containing media for several minutes. For larger probes, such as proteins conjugated to organic dyes, cell penetrating peptides (CPP) has been used to allow certain proteins to enter the cell [4]. In particular, poly-arginine has been used to introduce free GFP into the cell [5]. Other CPPs have shown to allow molecular entry of proteins, but is unclear whether the molecule entered are trapped in endosomes. CPP has been reported to bring in large molecule, such as quantum dot nanocrystals [6]. However, there hasn't been any report of specific labeling using quantum dots delivered by this method, as most of the uptakes are due to endocytosis and the delivered quantum dots are trapped in endosomes.

Mechanically injecting probes, or creating pores on the cell membrane using mechanical or chemical means are applied if the use of cell impermeant probes can't be avoided. Nano-injection method has been used to bring in small probes for performing super-resolution fluorescence microscopy [7]. There are several drawbacks with the injection methods. It is known to create structural artifact on actins at the point of injection. Second, microinjection provides entry into the cell, but it doesn't provide an exit for the free probe to be washed away. Therefore, the concentration of the probes injected should be very well optimized, otherwise a significant amount of unlabeled probes will be observed. The amount of probes required for injection method is also significantly higher; typically several micromolar concentration of probe is used for staining. Electroporation or microporation is another alternative to physically open holes on the membrane using electric current [8]. To ensure even permeabilization across all cells, it is often

necessary to detach adherent cells to suspension in order to make sure the cells are exposed to the electric field evenly. For imaging, the cells are then plated onto a coverslip after electroporation, which could take up to hours to attach depending on the cell type. This limits the time when one can start observing the kinetic of labeled protein to several hours after delivery of the probes. Osmotic pinosome lysis is a technique that is commercially available for delivering fluorescent probes inside the living cell [9]. The technique utilizes the formation of pinosomes, which formed by changing the osmolarity of the surrounding media. The cells are first exposed to a hypertonic solution along with the probe of interest. Pinosomes will then form on the cell membrane from probes that are intercalated in the membrane. The cells are then exposed to hypotonic solution, which lysis the pinosomes on the internal side of the cell membrane, breaking free the probes that were stuck. This method however is more applicable to probes that sticks to the cell membrane. Not to mention that the osmotic shock can often cause blebbing of the membrane, in which the cells do not recover from, and eventually lead to compromised membrane, or cell death. Recently, there is a new technique to deliver probes and large cargoes into the cell by using a photonic device [10]. The cells are cultured on a specialized coverslip, which causes bombardment of the cell membrane when exposed to laser light. The probes are then delivered into the cell during the period of membrane bombardment, when the holes are formed on the membrane. Using this technique, the authors were able to deliver cargo up to the size of *E.coli* that is micron in size. This technique is feasible but normally inaccessible to labs that doesn't have the specialized coverslip and instrumentation. Chemical means of creating holes on the cell membrane have been made possible by the use of pore-forming toxins [11]. Different toxins is known to create different sized holes; for instance, Streptolysin S creates holes that are permeable to molecules that are ~4.5 nm in diameter, whereas Streptolysin O

(SLO) makes the cell permeable to particles that are ~13 nm in diameter [12]. In particular, the large size of pore that SLO create makes it an idea candidate to use to introduce fluorescent probes into the cell.

1.2 STREPTOLYSIN O AND RELATED PORE FORMING TOXINS

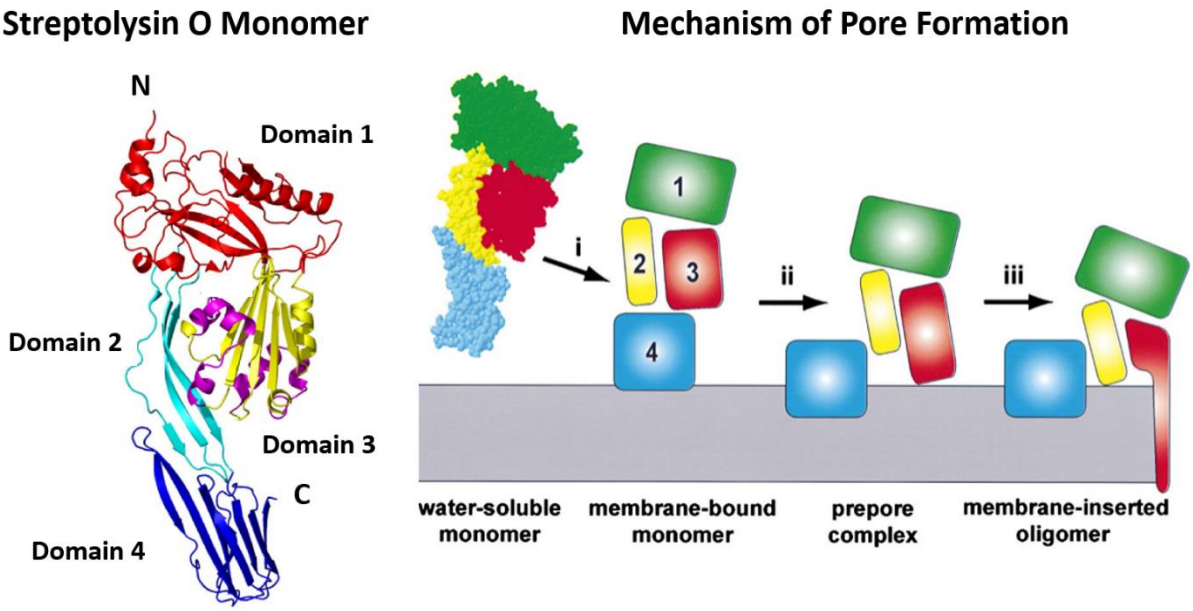

Figure 1.1. Crystal Structure of Perfringolysin O, which is only a few amino acid sequence different from Streptolysin O, and the mechanism of pore formation. The monomer consists of four domains. Right image from[13], and left image from[14].

Streptoysin O (SLO) is a 70 kDa bacterial enzyme that oligomerizes and forms pore on the cell membrane [11,15]. In general, the cholesterol binding cyclotoxins, such as Perfringolysin O and Streptolysin O consists of 4 domains (Fig 1.1). Domain 4 is hypothesized to be mostly responsible for membrane binding, whereas domain 1 and 3 are responsible for oligomerization and pore formation. Numerous studies have shown SLO, like other cholesterol binding cyclotoxins, binds to the cholesterol rich region on the membrane [14]. The oligomerization

process however, is still unclear at this point. For instance, the exact number of monomers per pore, and whether this number changes with concentration of the toxin and cholesterol content of the membrane is not yet known. A similar pore-forming toxins pneumolysin forms pore on the cell membrane with 30-50 monomers. A 3D reconstruction image of the pore complex based on cryo-EM data of pneumolysin is shown in Fig. 1.2.

Figure 1.2. 3D Reconstruction of the Oligomer Pore-Complex based on Cryo-EM data.

The sizes of pores that SLO forms can vary to a certain extend. For example, SLO has been shown to form pores that are arc like instead of complete circle, due to partial oligomerization [16]. What remains a mystery is the fact that although the pores are roughly 30-40 nm as shown by electron microscopy and AFM [16,17] (Fig. 1.3), the largest size of recorded molecule that enter or exit the cell is only ~13 nm in diameter[12]. The discrepancy of these experiments can be attributed to the use of different techniques. For instance, in EM and AFM, the cells are often fixed after pore formation, and the cells could have been permeabilized to a point of no return. It is possible that to remain cell viability, pore as large as 30-40 nm was never achieved and only smaller holes are formed. It is also unclear whether the SLO damage becomes irreversible is due to formation of too many pores, or formation of too large of a pore. More

studies are needed in order to elucidate the relationship between SLO concentration, pore size, and cell death.

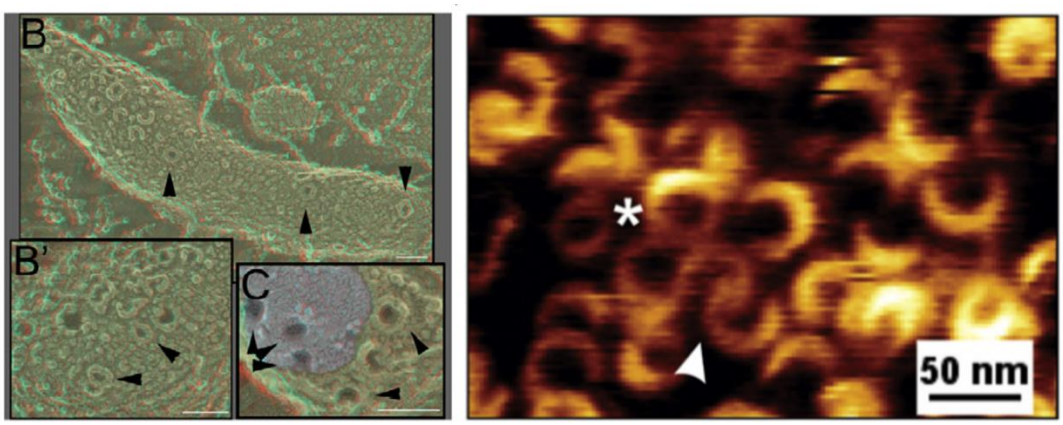

Figure 1.3. Image of the cell membrane pore complex based on electron microscopy and AFM imaging.

It is well known in literature that the pores formed by SLO on the membrane are eventually removed by the cell under a certain conditions, and the cells are viable after a brief period of recovery. However, there has been an inconsistency in how to initiate the recovery of SLO permeabilized cells, as well as how the cells even clear the numerous SLO pore complex off the cell membrane. Some studies mentioned the importance of calcium in membrane repair after SLO permeabilization [18]. Others used complete medium supplemented with FBS for recovery [19,20]. Some paper even further suggest the use of cytosolic solution from other cells to supplement the recovery process [21]. All of these studies provided proofs that the membrane has repaired, however, it is unclear whether incomplete oligomerization has occurred as mentioned before, and whether different degrees of permeabilization requires different recovery agents. The exact mechanism of how the cell membrane is repaired from these numerous pores is still controversial. One study suggests that the SLO oligomer is removed from the cell by bleb formation[17], while another study suggests that the oligomer is endocytosed inside the cell during

membrane repair[22]. Once again, more studies are needed in order to further understand the recovery mechanism of cells permeabilized by SLO.

Even though the pore formation and recovery mechanism of SLO are not well understood, experimentally SLO has been used to deliver DNA[23], RNA[19], ligands[24] and proteins[25],[26] into living cells. SLO was first shown to be able to cause reversible permeabilization of the membrane to a wide variety of proteins by Walev et al. [25]. Walev et al. showed that after SLO treatment, the cells were permeable to FITC labeled albumin and Fab'2 fragments. The purpose was to show that the membrane could be made permeable, and hence they did not show specific labeling from the delivered fluorescent molecules. In addition, the report claimed that the cells were only permeable up to 100 kDa of protein (Fab'2) and therefore excluded the possibility of bringing in primary antibodies such as IgG's that are ~150 kDa. Others have reported the entrance of macromolecules (>100 kDa) using SLO but did not provide evidence of specific labeling (for instance, colocalization with expressed fluorescent protein on the same target) and cell health, since the cells were either fixed immediately after delivery or cell viability at this permeabilization condition was never evaluated [9,18]. SLO has, however, been successfully used in live untransfected cells to deliver fluorescent probes bound to DNA and RNA, (including molecular beacons)[20] and the dynamic of mRNA are sometimes observed. There has yet to be any report of dynamic observation in proteins labeled by SLO permeabilization. Our goal is to use this technique to deliver a variety of fluorophores that are capable of providing superb photostability for observing the dynamic of proteins inside the living cell.

1.3 SINGLE DOMAIN ANTIBODY-A NOVEL CLASS OF FLUORESCENT PROBE

In general with pore-forming toxin permeabilization, small molecules are more permeable than large molecules [12]. It is therefore more efficient to deliver smaller probes into the cell if massive labeling of the cellular structure is desired. Although the delivery of full size antibody may be possible, to deliver enough antibody to stain a whole cellular structure can be challenging. An alternative to full antibody is to use single domain antibody for labeling cellular structure, which has been shown to be capable of doing this task by using the transfected cell to express recombinant single domain antibody labeled fluorescent protein [27]. A recent report has also successfully collected super-resolution images with dye labeled single domain antibody on fixed cells [28]. The single domain antibody, also termed nanobody, is a 15 kDa fragment antibody produced by llamas (Fig 1.4.).

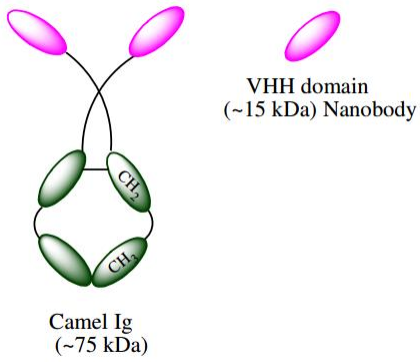

Figure 1.4. Single domain nanobody derived from camelid Immunoglobulin.

The library for single domain nanobody is still growing, but there has been reliable commercial source for nanobody against GFP, RFP, and few other proteins. It has been shown that GFP nanobody can be conjugated to compact quantum dots for immunolabeling of receptors

in the narrow synapses due to its size advantage [29]. GFP and RFP nanobody (GBP, RBP) can also be used as boosters for fluorescence signal (Fig. 1.5).

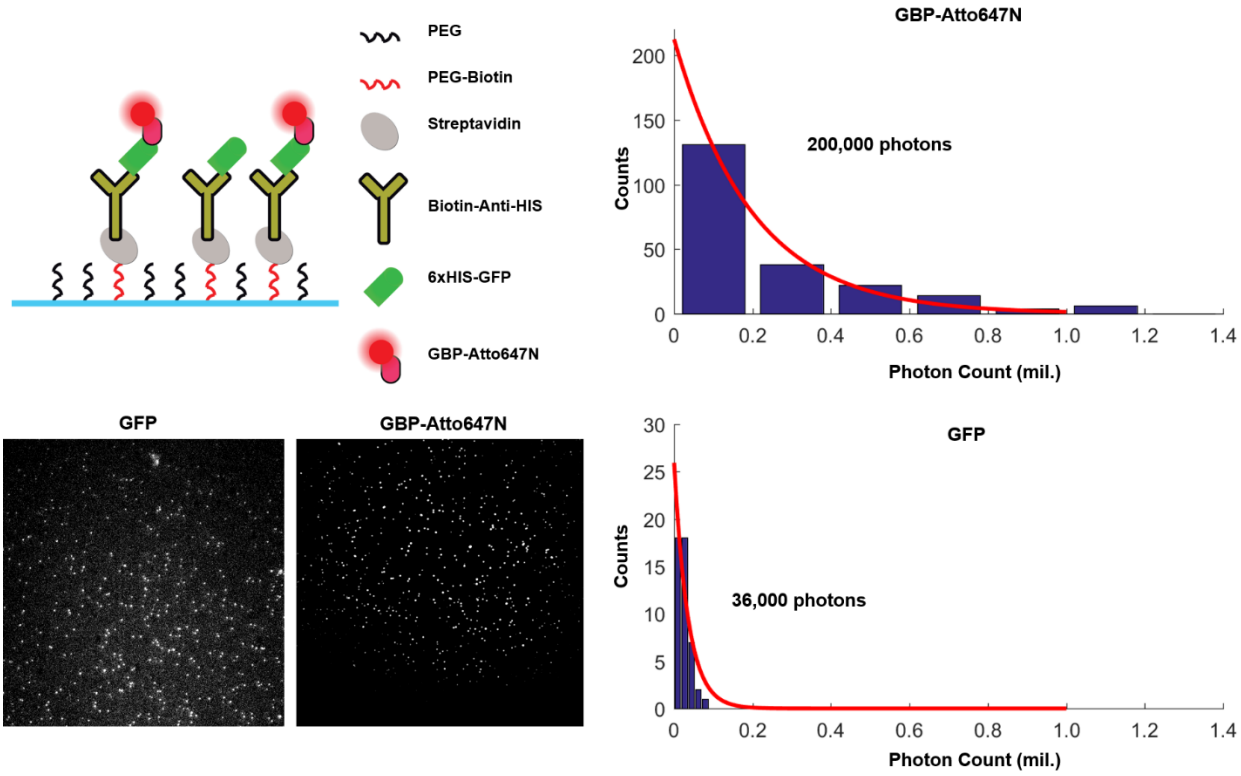

Figure 1.5. Total photon output of GFP versus Atto647N. Single molecules of GFP are measured by immobilizing GFP on glass. GFP was subsequently labeled by GBP-Atto647N. The total photon output of GFP and Atto647N are calculated.

In this example, GFPs are immobilized onto a glass coverslip and single molecule fluorescence images of GFP and GBP-Atto647N were collected until all the spots are photobleached. The total photon output of GFP before photobleaching was calculated, where we got an average of about 35,000 photons for the GFPs. After labeling the GFP with GBP-Atto647N, the total photon output increased to 200,000 photons, attributed to the photostability of Atto647N. This ~6x boost in photon output is very valuable for tracking molecular motors and imaging long time dynamics. In summary, the compact size of GBP, and ability to use it to boost

the fluorescence signal over existing fluorescent proteins, such as GFP and RFP makes it a very unique and useful class of probes to deliver inside the cell for single molecule tracking purposes.

1.4 DYNAMIC OF KINESIN-1 MOTOR IN VIVO

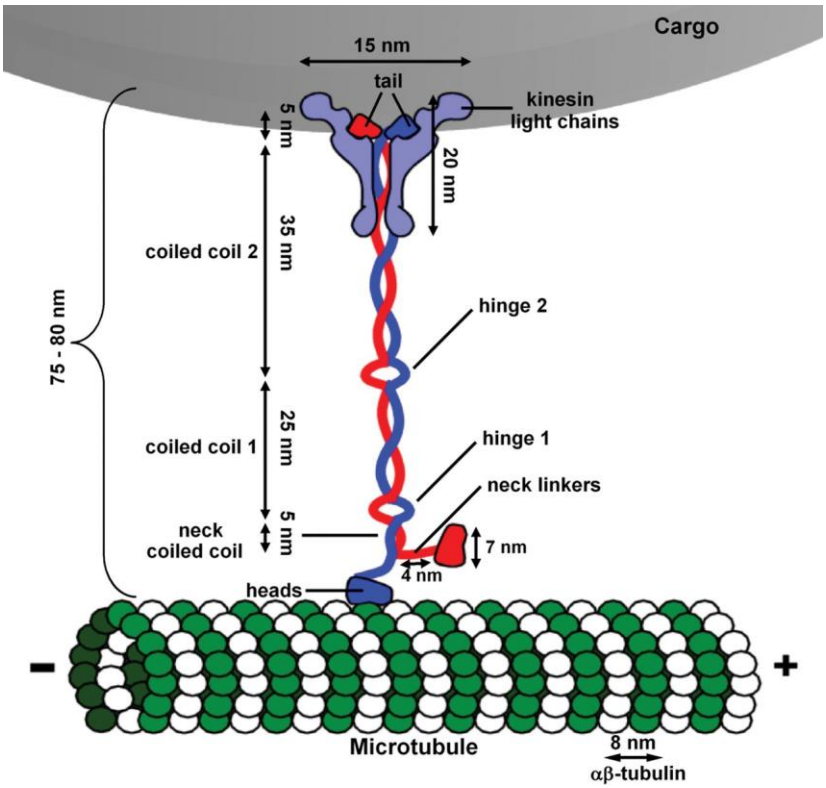

Figure 1.6. Structure of Full Length Kinesin 1. Image from http://www.biochemsoctrans.org/content/40/2/438.

Kinesin-1 is a plus end directed microtubule motor responsible for cargo transport in cells [30]. For each ATP hydrolyzed, kinesin "walks" 8 nm step, which is roughly the size of the tubulin dimer that the kinesin walks on. Naturally, kinesin exists as a homodimer, and the structure mainly contains two motor domains (or heads), and a long stalk (Fig 1.6). Kinesin has been reported to mostly be in-active *in vivo* due to the folding of hinge 2, and the interaction between cargo binding domain and the motor domain. Therefore, various constructs of kinesins have been made to eliminate the motility issue due to in-activation so that they can be better studied. This is

typically done by truncating the kinesin above hinge 1. Although kinesin has been studied extensively *in vitro*, very little is known about its biophysical properties *in vivo*. Numerous paper has reported that when tracking cellular vesicles, such as in the long axon of neurons, the velocity of kinesin can be several microns per second, and the cargo also exhibit extremely long run length [31,32]. Through *in vitro* measurement, it is well known that the velocity of kinesin is roughly under a micron per second (depending on temperature, type of buffer used, and other factors), and the run length of individual motor is about a micron in length[33]. The big question now is whether the increase in velocity and run length that have been measured from vesicles is due to the intracellular condition of being *in vivo*, or is the elevated speed caused by other proteins that attached to the kinesin and cargo, which the kinesin was carrying and caused the increase in speed. All these questions cannot be answered until we're able to measure and study the properties of kinesin molecule *in vivo*. The difficulty in studying single molecular motors *in vivo* is the fact that currently there isn't a way to label the motor proteins in cells with a photostable dye. This problem can be circumvented by appending FP to the molecular motor. However, kinesin fused to fluorescent proteins photobleaches extremely fast and suffers from poor signal to noise in the intracellular environment. An interesting attempt to solve this problem is by using kinesin fused to tandem fluorescent proteins (FP) [34]. This particular study done by Verhey lab was able to measure the velocity of kinesin inside the cell, by increasing the photon output high enough to track individual kinesin via its 6 FP tags. However, it is very challenging to obtain the exact expression level where individual kinesin can be observe, as the cells typically over-expresses transiently transfected proteins. Just within hours, the cells could be filled with the protein of interest. It was also reported that this tandem FP fusion kinesin construct are not all functional. For instance, they have observed that the kinesin with a shorter

stalk region (K560) aren't functional after the attachment of three FPs. SLO permeabilization is a great way to overcome this problem by introducing fluorescent probes that are specific to the kinesin, and increase photon output of the FP attached by using the nanobody probes mentioned above.

1.5 SUPER-RESOLUTION MICROSCOPY WITH DELIVERED FLUORESCENT PROBE

Recently super-resolution microscopy that utilizes localization of single fluorophore has been very popular [35]. The technique, such as stochastic optical reconstruction microscopy (STORM) uses the detection of isolated fluorophores per frame to construct an overall high resolution image of the cell, where each molecule is localized to roughly 10-20 nm accuracy (Fig. 1.7). Such technique requires either the use of a photoswitchable probe, or a probe that can activated stochastically, so that the probes can be turned on/off to have a chance of detecting isolated molecules.

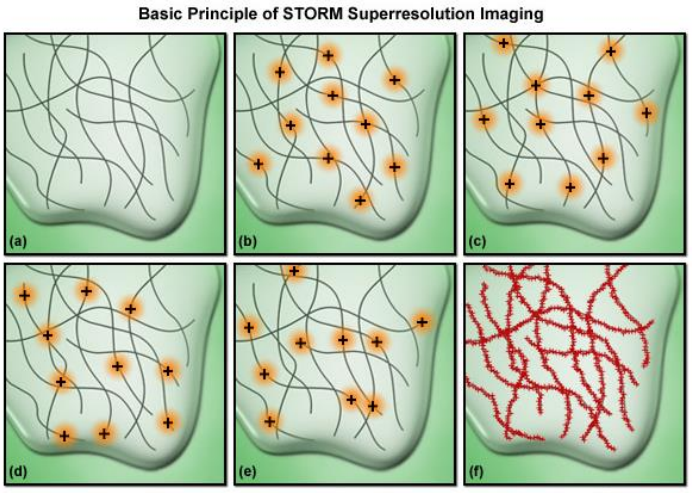

Figure 1.7. Basic Principle Behind Stochastic Optical Reconstruction Microscopy (STORM).

http://microscopyu.com/tutorials/flash/superresolution/storm/index.html

Typically, the dyes are deactivated with the aid of reducing agent, like sodium borohydrate, BME, MEA, or glutathione [36]. Because photobleaching limits the number of cycles a particular dye can be activated, typically an oxygen scavenging system, such as glucose oxidase/catalase + glucose, or PCD/PCA are used. So far, super-resolution techniques like these have huge success in revealing detailed cytoskeleton structures such as microtubule and actin in fixed cells [36,37]. A comprehensive review has been published evaluating different fluorophores and their potential to be used for direct STORM (dSTORM)[38]. The concept of dSTORM is similar to STORM, but the use of an activator dye is not necessary; the fluorophore undergoing photoswitching on its own in the presence of thiol containing reducing agent. Unfortunately, most of these probes that they find extremely efficient for dSTORM, such as Cy3B and Alexa647 are cell impermeant, which limits the use of the technique on live cells. Potentially what we want to do with our technique is to be able to deliver these dSTORM probes inside the cell, so that dSTORM can be performed on living cells.

1.6 REFERENCES

1. Los, G. V. *et al.* HaloTag: A Novel Protein Labeling Technology for Cell Imaging and Protein Analysis. *ACS Chem. Biol.* **3,** 373–382 (2008).
2. Keppler, A. *et al.* A general method for the covalent labeling of fusion proteins with small molecules in vivo. *Nat. Biotechnol.* **21,** 86–89 (2003).
3. Gallagher, S. S., Sable, J. E., Sheetz, M. P. & Cornish, V. W. An In Vivo Covalent TMP-Tag Based on Proximity-Induced Reactivity. *ACS Chem. Biol.* **4,** 547–556 (2009).

4. Richard, J. P. *et al.* Cell-penetrating Peptides A REEVALUATION OF THE MECHANISM OF CELLULAR UPTAKE. *J. Biol. Chem.* **278,** 585–590 (2003).
5. Jo, J., Hong, S., Choi, W. Y. & Lee, D. R. Cell-penetrating peptide (CPP)-conjugated proteins is an efficient tool for manipulation of human mesenchymal stromal cells. *Sci. Rep.* **4,** (2014).
6. Liu, B. R., Huang, Y.-W., Chiang, H.-J. & Lee, H.-J. Cell-Penetrating Peptide-Functionized Quantum Dots for Intracellular Delivery. *J. Nanosci. Nanotechnol.* **10,** 7897–7905 (2010).
7. Hennig, S. *et al.* Instant Live-Cell Super-Resolution Imaging of Cellular Structures by Nanoinjection of Fluorescent Probes. *Nano Lett.* **15,** 1374–1381 (2015).
8. Kim, J. A. *et al.* A novel electroporation method using a capillary and wire-type electrode. *Biosens. Bioelectron.* **23,** 1353–1360 (2008).
9. Ahnert-Hilger, G., Bader, M. F., Bhakdi, S. & Gratzl, M. Introduction of macromolecules into bovine adrenal medullary chromaffin cells and rat pheochromocytoma cells (PC12) by permeabilization with streptolysin O: inhibitory effect of tetanus toxin on catecholamine secretion. *J. Neurochem.* **52,** 1751–1758 (1989).
10. Wu, Y.-C. *et al.* Massively parallel delivery of large cargo into mammalian cells with light pulses. *Nat. Methods* **12,** 439–444 (2015).
11. Alouf, J. E. in *Pore-Forming Toxins* (ed. Goot, P. F. G. van der) 1–14 (Springer Berlin Heidelberg, 2001).
12. Buckingham, L. & Duncan, J. L. Approximate dimensions of membrane lesions produced by streptolysin S and streptolysin O. *Biochim. Biophys. Acta* **729,** 115–122 (1983).

13. Feil, S. C., Ascher, D. B., Kuiper, M. J., Tweten, R. K. & Parker, M. W. Structural Studies of Streptococcus pyogenes Streptolysin O Provide Insights into the Early Steps of Membrane Penetration. *J. Mol. Biol.* **426,** 785–792 (2014).
14. Heuck, A. P., Hotze, E. M., Tweten, R. K. & Johnson, A. E. Mechanism of membrane insertion of a multimeric beta-barrel protein: perfringolysin O creates a pore using ordered and coupled conformational changes. *Mol. Cell* **6,** 1233–1242 (2000).
15. Bhakdi, S., Roth, M., Sziegoleit, A. & Tranum-Jensen, J. Isolation and identification of two hemolytic forms of streptolysin-O. *Infect. Immun.* **46,** 394–400 (1984).
16. Stewart, S. E. *et al.* Assembly of streptolysin O pores assessed by quartz crystal microbalance and atomic force microscopy provides evidence for the formation of anchored but incomplete oligomers. *Biochim. Biophys. Acta BBA - Biomembr.* **1848,** 115–126 (2015).
17. Keyel, P. A. *et al.* Streptolysin O clearance through sequestration into blebs that bud passively from the plasma membrane. *J. Cell Sci.* **124,** 2414–2423 (2011).
18. Boyle, R. T. & Lieberman, M. Permeabilization by streptolysin-o reveals a role for calcium-dependent protein kinase c isoforms alpha and beta in the response of cultured cardiomyocytes to hyposmotic challenge. *Cell Biol. Int.* **23,** 685–693 (1999).
19. Brito, J. L. R., Davies, F. E., Gonzalez, D. & Morgan, G. J. Streptolysin-O reversible permeabilisation is an effective method to transfect siRNAs into myeloma cells. *J. Immunol. Methods* **333,** 147–155 (2008).
20. Nitin, N. & Bao, G. NLS peptide conjugated molecular beacons for visualizing nuclear RNA in living cells. *Bioconjug. Chem.* **19,** 2205–2211 (2008).

21. Kano, F., Nakatsu, D., Noguchi, Y., Yamamoto, A. & Murata, M. A Resealed-Cell System for Analyzing Pathogenic Intracellular Events: Perturbation of Endocytic Pathways under Diabetic Conditions. *PLOS ONE* **7,** e44127 (2012).
22. Corrotte, M., Fernandes, M. C., Tam, C. & Andrews, N. W. Toxin pores endocytosed during plasma membrane repair traffic into the lumen of MVBs for degradation. *Traffic Cph. Den.* **13,** 483–494 (2012).
23. Giles, R. V. *et al.* Selecting optimal oligonucleotide composition for maximal antisense effect following streptolysin O-mediated delivery into human leukaemia cells. *Nucleic Acids Res.* **26,** 1567–1575 (1998).
24. Kano, F., Sako, Y., Tagaya, M., Yanagida, T. & Murata, M. Reconstitution of brefeldin A-induced golgi tubulation and fusion with the endoplasmic reticulum in semi-intact chinese hamster ovary cells. *Mol. Biol. Cell* **11,** 3073–3087 (2000).
25. Walev, I. *et al.* Delivery of proteins into living cells by reversible membrane permeabilization with streptolysin-O. *Proc. Natl. Acad. Sci. U. S. A.* **98,** 3185–3190 (2001).
26. Wu, J. & Berland, K. M. Comparing the intracellular mobility of fluorescent proteins following in vitro expression or cell loading with streptolysin-O. *J. Biomed. Opt.* **13,** 31214 (2008).
27. Rothbauer, U. *et al.* Targeting and tracing antigens in live cells with fluorescent nanobodies. *Nat. Methods* **3,** 887–889 (2006).
28. Ries, J., Kaplan, C., Platonova, E., Eghlidi, H. & Ewers, H. A simple, versatile method for GFP-based super-resolution microscopy via nanobodies. *Nat. Methods* **9,** 582–584 (2012).
29. Cai, E. *et al.* Stable Small Quantum Dots for Synaptic Receptor Tracking on Live Neurons. *Angew. Chem.* **126,** 12692–12696 (2014).

30. Hirokawa, N., Noda, Y., Tanaka, Y. & Niwa, S. Kinesin superfamily motor proteins and intracellular transport. *Nat. Rev. Mol. Cell Biol.* **10,** 682–696 (2009).
31. Schwartz, J. H. Axonal Transport: Components, Mechanisms, and Specificity. *Annu. Rev. Neurosci.* **2,** 467–504 (1979).
32. Allen, R. D., Metuzals, J., Tasaki, I., Brady, S. T. & Gilbert, S. P. Fast axonal transport in squid giant axon. *Science* **218,** 1127–1129 (1982).
33. Norris, S. R., Núñez, M. F. & Verhey, K. J. Influence of Fluorescent Tag on the Motility Properties of Kinesin-1 in Single-Molecule Assays. *Biophys. J.* **108,** 1133–1143 (2015).
34. Tracking Single Kinesin Molecules in the Cytoplasm of Mammalian Cells. Available at: http://www.sciencedirect.com/science/article/pii/S000634950771216X. (Accessed: 9th May 2016)
35. Yildiz, A. *et al.* Myosin V Walks Hand-Over-Hand: Single Fluorophore Imaging with 1.5-nm Localization. *Science* **300,** 2061–2065 (2003).
36. Vaughan, J. C., Jia, S. & Zhuang, X. Ultrabright photoactivatable fluorophores created by reductive caging. *Nat. Methods* **9,** 1181–1184 (2012).
37. Xu, K., Zhong, G. & Zhuang, X. Actin, spectrin and associated proteins form a periodic cytoskeletal structure in axons. *Science* **339,** (2013).
38. Dempsey, G. T., Vaughan, J. C., Chen, K. H., Bates, M. & Zhuang, X. Evaluation of fluorophores for optimal performance in localization-based super-resolution imaging. *Nat. Methods* **8,** 1027–1036 (2011).

Chapter 2

Material and Methods

2.1 MAMMALIAN CELL CULTURE

SLO permeabilization experiments conducted on various mammalian cell lines. The cell lines tested included CHO-K1, COS-7, HeLa, U2OS, and NSC34. A table for culture media and doubling time for each of the cell line is below:

Cell line	Culture Media	Doubling Time
CHO-K1	F12K 10% FBS PS	16 hrs
COS-7	DMEM 10% FBS	18 hrs
HeLa	MEM 10% FBS PS	24 hrs
U2OS	DMEM 10% FBS PS	29 hrs
NSC34	DMEM 10% FBS PS	Not Available

Table 2.1. Culture media for cell lines maintained for SLO experiments along with their doubling time. PS= penicillin streptomycin

Cells are cultured in 25 mm filtered flask, and subcultured whenever the cells reach ~90% confluency. Subculture protocol is described below:

-Wash cells with PBS 3x

-Add 2 mL 0.25% Trypsin-EDTA (Gibco or Corning), incubate for 5" in 37 degree C 5% CO_2 incubator.

-Check the cells under microscopy to make sure they're rounded up, which means the cells are detached from the surface of the flask.

-Neutralize the 0.25% Trypsin-EDTA with 6 mL complete medium for the particular cell line.

-Dilute cells anywhere between 1:10 to 1:4 ratio by diluting the cell solution with complete medium. For CHO-K1 cells or fast growing cells 1:10 ratio is used, whereas for slow growing cell such as U2OS cells, 1:4 ratio is used.

-After the cells are transferred to a new flask, gently mix the cells by swirling the flask in figure 8 pattern.

2.2 GFP NANOBODY EXPRESSION PURIFICATION

The protocol for purifying recombinant nanobody GBP (GFP binding protein) is detailed below:

-Plate bacteria from BL21+GBP plasmid Glycerol stock in -80C (DO NOT THAW THE GLYCEROL STOCK) by dipping a 100 uL pipet tip deep into the frozen glycerol and then streak LB plate with KANAMYCIN using the pipet tip or a new streaking stick. Allow the colonies to form overnight.

-Pick one colony from the plate and start overnight culture in 50 mL LB + kanamycin in a shaker at 37 degree C.

-Add 5 mL of overnight culture into each 1 L flask containing LB + kanamycin, grow until OD reaches 0.6 to 1.5 in 37 degree C shaker. Save a sample of bacteria when O.D. reaches 0.6 for gel verification.

-Add final concentration of 0.5 mM IPTG into each flask, express the protein at room temperature while shaking with the lid open for 4 hours.

-Save a small amount of bacteria for gel verification. Harvest the bacteria by centrifuging the bacteria at 6000g and 4 degree C for 15 minutes using a GSA rotor (Sorvall).

-Discard the LB, store pellet in -80 until ready to start lysis/protein purification.

-Prepare Purification buffer (PB):

50 mM NaH_2PO_4/$NaHPO_4$ (pH 8)

250 mM NaCl

1 mM $MgCl_2$

Take the above buffer, prepare a separate buffer containing 500 mM imidazole (PBI) adjust pH to 8 with HCl.

-Prepare Lysis buffer

50 mM Imidazole in PB by mixing ratios of PB + PBI. (dilute PBI 10x with PB)

1 mg/mL lysozyme

250 uL Protease inhibitor cocktail for his-tagged protein (Sigma)

1 mM PMSF (100 mM PMSF in isopropanol)

15 ug/mL Benzamydine (15 mg/mL Benzamidin in ddH20)

-Once the buffers are prepared, dissolve bacteria pellet in Lysis buffer (~35 mL for 2 L flasks).

-Add 1 scoop full of DNase. Incubate the lysing bacteria on ice for 15 minutes.

-Sonicate the bacteria in lysis buffer at 40% amplitude for 60s (10s on/10s off)

-Centrifuge cell lysate at 15,000g 4C for 20 minutes using Beckman coulter ultracentrifuge.

-During centrifugation, prepare NiNTA resin by discarding the original solution, wash it with at least 10 mL ddH20, and then equilibrate it with 50 mM Imidazole PB (by mixing PB and PBI). I used ~2.5 mL of resin for 2L culture. Leave ~1 mL of 50 mM imidazole buffer in the resin.

-After bacteria lysate is centrifuged, collect the supernatant but be careful not to disturb the pellet.

-Incubate the collected supernatant with the NiNTA resin while shaking for 1.5 hours at 4 degree C.

-At the end of 1.5 hour pour the content (NiNTA + lysate) in the column, and collect flow through.

-Wash the column with 50 mM imidazole buffer. The volume of buffer needed depends on whether protein is still present in the flow through. I run a qualitative Bradford assay concurrently as I purify to make sure all the unwanted proteins are washed away.

-During the wash prepare subsequent buffer, 100 mM imidazole buffer is next. Prepare this from PB and PBI.

-GBP should come out at 150 mM imidazole prepare 10 mL of 150 mM imidazole buffer, and collect 2, 4, 4 mL for 3 fractions. Concurrent Bradford assay will help you check when the protein starts to come out. For Bradford Assay protocol, see below.

-Collect another flow through with 10 mL 250 mM Imidazole towards the end of 250mM elution, no more protein should come out.

-Run a SDS gel to check purity and concentration of protein (see Figure 2.1).

Figure 2.1 SDS-PAGE Gel of Purified GBP. Purified GBP appears as a 15 kDa band on the gel.

-Pure GBP fraction were collected, in my case 150 mM fraction 2 and 3, do Bradford assay to check concentration, and dilute the protein to below 100 uM (~50 uM recommended).

-flash freeze and stored protein in -80 degree C freezer. 2 L of LB yielded roughly 8mL of 70 uM of GBP (fraction 2&3 + diluted 2x further with PB)

Protein concentration determination with Bradford Assay:

Reagents needed:

-Bradford assay reagent (also called Coomassie G-250) from Bio-rad

-Protein Calibration Standard (Usually Bovine serum albumin, BSA)

-Molecular Biology Grade Water

Protocol:

1. Dilute Bradford Assay Reagent to 1X in Molecular Biology Grade Water, its usually a 5x dilution.

2. Establish a Bradford Assay calibration curve by adding 2 uL of various concentration of BSA at 2, 1.5, 1, 0.5, 0.25, 0 mg/mL to 100 uL of Bradford Assay reagent. Measure the O.D. at 595 nm after waiting 10 minutes. Result should be roughly linear between O.D. and protein concentration, see Fig. 2.2 below.
3. Calculate the protein concentration of your protein of interest using the calibration curve established.

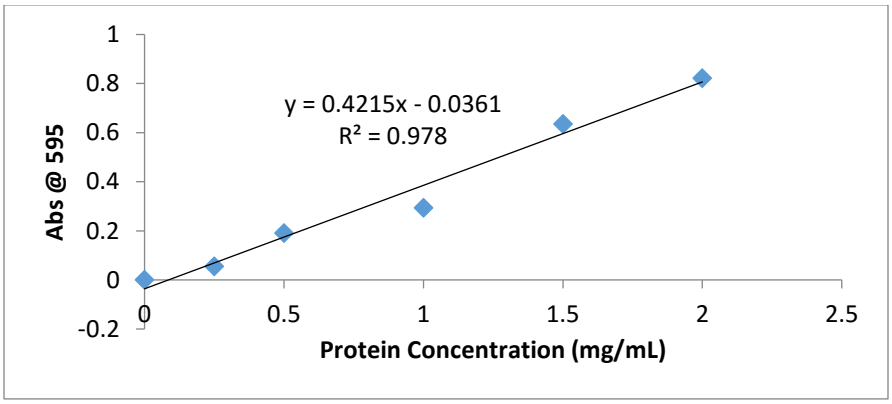

Figure 2.2. Bradford Assay Calibration Curve using BSA. Absorbance at 595 nm was measured for BSA in the concentration of 2 mg/mL, 1.5 mg/mL, 1 mg/mL, 0.5 mg/mL and 0.25 mg/mL.

2.3 PROTEIN LABELING AND PURIFICATION

To prepare for probes used in the study, nanobody such as GBP, or commercially available primary antibody has to be labeled by organic dyes. Generally the labeling strategy we use is to label the amine groups on protein with NHS-ester-organic dye. The protocol is described below:

Reagents needed:

-Primary antibody or nanobody at 0.1 mg/mL – 1.0 mg/mL in PBS

-Organic dye with NHS-ester (lyophilized)

-1 M Sodium Bicarbonate

-3500 mw cutoff desalting column

Protocol:

1. Add 1/10 volume of 1 M Sodium Bicarbonate to antibody solution to adjust pH.
2. Dissolve organic dye NHS-ester in DMSO at 10 mg/mL.
3. Add minimum amount of dissolved dye to antibody so that the ratio between antibody and dye is 6:1 for primary antibody, and 3:1 for nanobody.
4. Incubate the dye and antibody for 2 hours at room temperature.
5. Purify the free dye away by passing the labeled protein through a 3500 mw cutoff desalting column.

2.4 MOLECULAR BIOLOGY: PCR AND SUBCLONING

Sub-cloning is necessary for preparing plasmids with additional insert fused to our protein of interest. For example, we often subclone plasmid to add a Halotag or GFP on our protein of interest. It also work for substituting an existing tag for another tag, such as changing an existing GFP to halotag and vice versa. The general strategy for sub-cloning is via the use of Gibson's assembly, which is described in the diagram below (Fig. 2.3).

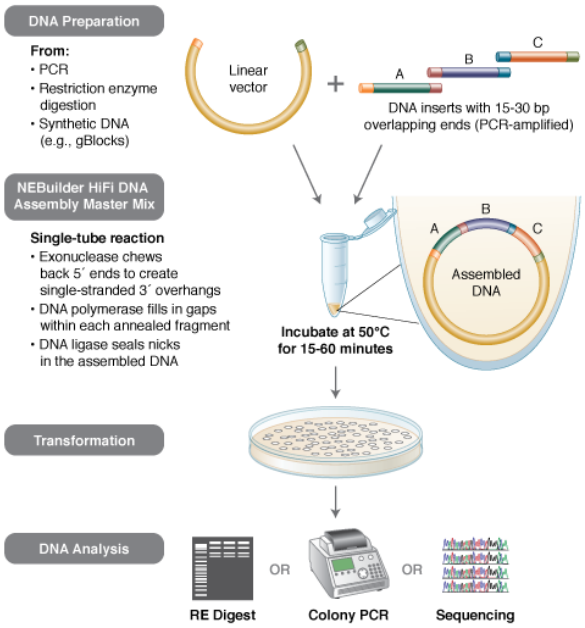

Figure 2.3. Schematic diagram of how sub-cloning via Gibson Assembly works. https://www.neb.com/products/e2621-nebuilder-hifi-dna-assembly-master-mix

The Gibson Assembly adds fragments of DNA to a linearized vector through overlaps at the two ends. PCR is used to create linearized vector and the DNA fragments. As an example, here is the protocol used to subclone a GFP into a p65-halotag plasmid. Here we wish to attach an eGFP insert at the C terminal end of the p65-halotag, resulting in a plasmid encoding for p65-halotag-GFP (Fig. 2.4).

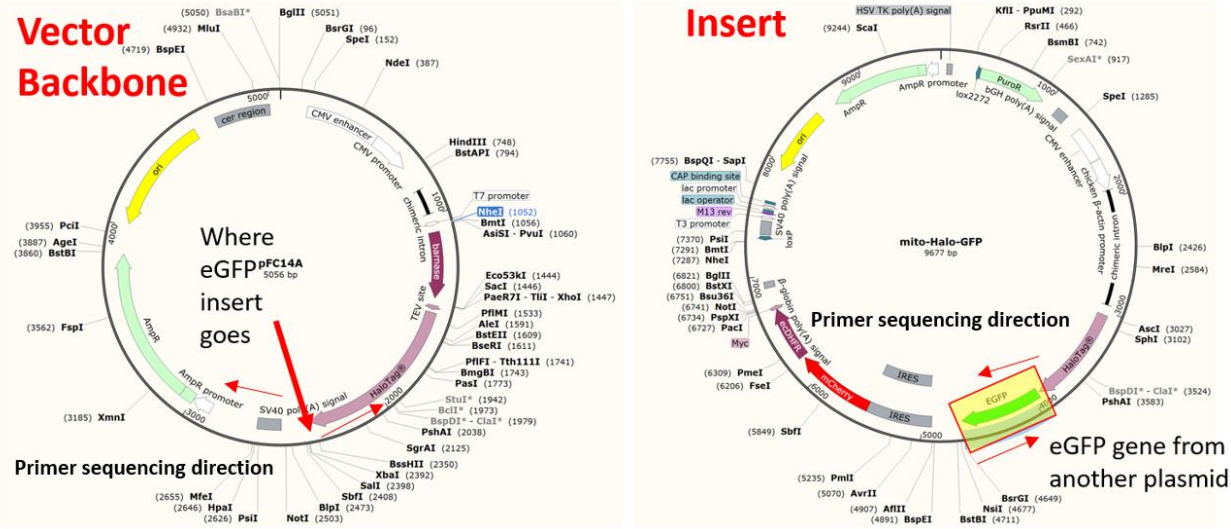

Figure 2.4. Example backbone plasmid and Insert with PCR sequencing direction.

To obtain linearized vector and the insert, we perform PCR on the two plasmid, each with 2 different primers. The primers for the linearized vector will bind to the left and right of the insertion site from 5' to 3' direction. The primers for the eGFP gene will bind at the two ends of the gene, but with an additional ~12 nt of overlap with the vector backbone next to the insertion site. An example of the primer design is shown below (Fig. 2.5).

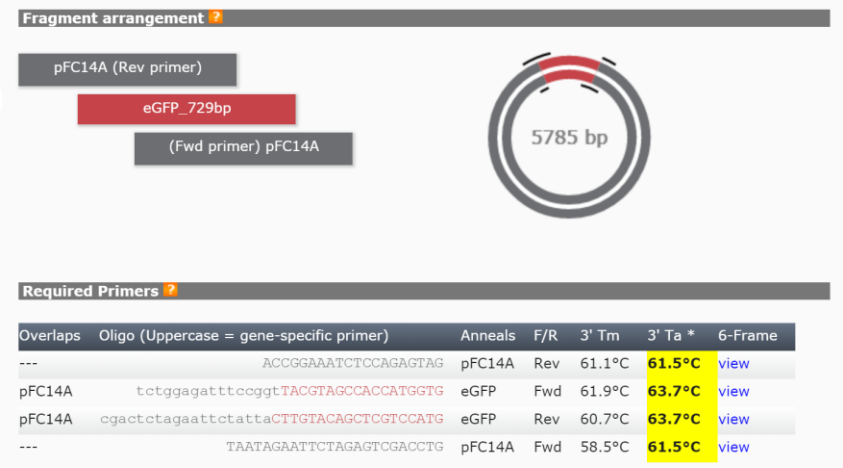

Overlaps	Oligo (Uppercase = gene-specific primer)	Anneals	F/R	3' Tm	3' Ta *	6-Frame
---	ACCGGAAATCTCCAGAGTAG	pFC14A	Rev	61.1°C	**61.5°C**	view
pFC14A	tctggagatttccggtTACGTAGCCACCATGGTG	eGFP	Fwd	61.9°C	**63.7°C**	view
pFC14A	cgactctagaattctattaCTTGTACAGCTCGTCCATG	eGFP	Rev	60.7°C	**63.7°C**	view
---	TAATAGAATTCTAGAGTCGACCTG	pFC14A	Fwd	58.5°C	**61.5°C**	view

Figure 2.5. Example of primer design. Primer for the insert needs to contain ~12 nt of overlap with the vector backbone. http://nebuilder.neb.com/

The red text are segment of primer that binds the insert eGFP gene, whereas the grey letters are the overlap that it create based on the neighboring sequence of the insertion site on the vector backbone. Once the primers design is finished, primer and be ordered and once arrived we proceeds with PCR.

The protocol for PCR is as follows:

Reagents needed:

-Phusion Hi-Fi PCR Kit (NEB)

-Primers (500 uM)

-10 ng/uL Plasmid DNA

-Molecular Biology Grade Water

Protocol:

1. To prepare a final volume of 50 uL PCR product, add the following in order:
2. 36.5 uL Molecular Biology Grade Water
3. 10 uL 5x Phusion HF Buffer
4. 1 uL 10 mM dNTPs
5. 0.5 uL Forward Primer
6. 0.5 uL Reverse Primer
7. 1 uL Template DNA
8. 0.5 uL Phusion Polymerase
9. Program the thermocycler with the following setting:
10. Initial denaturation: 98 degree C for 30 seconds
11. 30x cycles of 98 degree C for 30 seconds, annealing temperate of your primers for 30 seconds (lower of the two), 72 degree C extension for 30 seconds per 1000 basepairs.

12. Final extension 72 degree C for 5 minutes

13. Hold at 4 degree C.

At the end of PCR, check the fragment sizes using 0.8% agarose gel (320 mg agarose in 40 mL 1X TAE Buffer (40 mM Tris, 20 mM Acetatic Acid, 1mM EDTA), plus 1X SYBR Safe Stain). The fragments are loaded along with 6x loading buffer (3mL glycerol, 25mg bromophenol blue, 7 mL ddH2O). Gel was ran at 120V for 50 minutes. At the end of the run, gel was visualized under UV light. Fragments should appear yellow. Once the fragments are verified to be the correct size, proceed to clean up the plasmid DNAs in the PCR products by doing DPNI Digest, where the methylated nucleotides on the plasmid DNA are cleaved. DPNI Digest is performed following the protocol below:

Reagents Required:

-DPN1 Enzyme 20,000 units/mL

-NEB Buffer #4

Protocol:

1. Add 4.6 uL NEB Buffer #4 and 1.75 uL DPN1 Enzyme to 40 uL PCR products
2. Incubate at 37 degree C for 2 hours
3. Heat inactivate at 80 degree C for 20 minutes

After the digest proceed with PCR cleanup. PCR cleanup was conducted by using PCR Cleanup Kit (Thermo Fisher) following manufacturer's protocol. With the purified PCR fragments and linearized vectors, we proceed on to forming Gibson Assembly using NEB Assembly Master Mix. Following the protocol below:

Reagents Required:

-2x NEB Assembly Master Mix

-PCR products (linear and insert)

-Molecule Grade Water

Protocol:

1. Put in (10-x) uL of DNA so that the total amount of DNA in terms of mass is between 0.03 – 0.2 pmol. Fill rest of the volume with water.
2. Put in 10 uL of 2x NEB Assembly Master Mix
3. Incubate the mixture at 50 degree C for 30 minutes. Keep it on ice afterward.
4. Add 2 uL of DNA assembled product to an aliquot of competent *E.coli* (DH5α). Incubate on ice for 30 minutes.
5. Heat shock the *E.coli*. at 42 degree C for 30 seconds.
6. Incubate bacteria on ice for 2 minutes.
7. Add 950 uL S.O.C. Medium, and put the bacteria in the shaker for 60 minutes at 37 degree C.
8. Plate 100 uL of cells on correct antibiotic resistance agar plate, and let it grow overnight at 37 degree C.
9. Grow and sequence 4-10 colonies on the agar plate the next morning to verify whether the subcloning was successful.

During the time we wait for sequencing, we usually run a gel to verify the number of basepairs in the new plasmids. We then just transfect the cell with the new plasmids to check the functionality of the new protein.

2.5 STREPTOLYSIN O PERMEABILIZATION PROTOCOL

Streptolysin O (SLO, 25,000-50,000 U, Sigma Aldrich) was dissolved in 1 mL of molecular biology grade water. The stock solution was aliquoted and stored at -80 ^{o}C freezer. A new aliquot was thawed prior to each experiment and used within 5 hr. The SLO stock solution was further diluted to working concentration in DPBS supplemented with 1 mM $MgCl_2$. Working SLO concentration was determined by testing a range of SLO concentrations for each cell line to achieve >75% permeability to 10 kDa fluorescein dextran. Different cell lines required different dosage of SLO; CHO-K1 required 250x dilution of the SLO stock, HeLa cell required 250x dilution, and U2OS cells required 500-1000x dilutions. A table of toxin concentration and incubation time for permeabilization using SLO is provided below.

Cell line	**Cell Confluency**	**Dilution of SLO stock (S5265)**	**SLO Inc. Time**
CHO-K1	90-100%	250x diluted	7 minutes
CHO-K1	80%	334x diluted	10 minutes
CHO-K1	65-70%	334x diluted	7 minutes
U2OS	80%	500x diluted	8 minutes
U2OS	50%	774x diluted	7 minutes
U2OS	30-40%	1000x diluted	7 minutes
HeLa	50-75%	250x diluted	10 minutes
COS7	50-75%	666x diluted	10 minutes
NSC34	50%	500x diluted	8 minutes

Table 2.2. Dilution table of concentration of SLO toxins and time required to permeabilize different cell lines at different confluency.

The cells grown to 80-100% confluency were incubated in SLO containing buffer for 7-10 min at 37 ^{o}C. Permeabilized cells can be observed under phase contrast microscopy at 20x magnification after 5 min. The granules inside the cells are more distinctive in permeabilized cells. Fluorescent probes were diluted in Tyrode's buffer without calcium (140 mM NaCl, 5 mM KCl, 1 mM $MgCl_2$, 10 mM HEPES, 10 mM glucose, pH 7.4). After SLO permeabilization, the cells were washed 2x with DPBS + 1 mM $MgCl_2$. The cells were fluorescently labeled by incubating with the probes, such as DAPI, chloroalkane-Alexa660 (Promega), phalloidin dye conjugate (Thermo-Fisher), nanobody-dye conjugate (Chromotek), and labeled IgG (Thermo-Fisher) at a final concentration of 300-700 nM for 5 min on ice. For preparation of haloligand SA probe, SA was incubated with biotin-PEG-chloroalkane at 1:6 molar ratio for 10 min. Free SA binding sites were then saturated with excess free biotin for 5 min. The sample was purified by using a desalting column (30 kDa MW cutoff, Amicon). If the probe is prone to cause non-specific binding on the coverslip or cell membrane, 2.5 L of 10X Casein (Vector Lab) was added to the Tyrode's buffer along with the probes. After labeling, the cells were washed 3x with Tyrode's buffer, and incubated with recovery medium (Phenol red (P/R) free DMEM with sodium pyruvate, 10% FBS, 2mM ATP, 2mM GTP, 2 mg/mL glucose, without antibiotic) for 20 min. To check whether the cell membrane has recovered, the cells were washed with PBS 3x, and incubated with 500 nM of 20 kDa Texas Red dextran diluted in DPBS 1 mM $MgCl_2$ for 5 min. As a negative control, another coverslip of cell underwent the same treatment except the addition of SLO were also imaged. The negative control was then exposed to SLO and consequently 20 kDa Texas Red dextran to show that the cells are permeant to 20 kDa Texas Red Dextran if the cell membrane was still permeable.

For transfection, all cells were transiently transfected with Lipofectamine 2000 (Life Technologies) following the manufacturer's protocol, with plasmid DNA (pERB254) encoding GFP-ActA-Halotag, which is a mitochondria membrane targeting protein, (pERB254 was a gift from Michael Lampson (Addgene plasmid # 67762)) or PCNA-GFP (a protein localized in nucleus). The transfection media was removed after 3 hours for human cell lines (HeLa, U2OS) which are sensitive to presence of lipofectamine. Unless specified otherwise, the permeabilization procedure was done on cells after protein expression takes place overnight. Post membrane recovery and before imaging, the cells were washed once with 10% FBS DMEM P/R free, and cells are imaged in 10% FBS DMEM P/R free medium at 30 degree C unless otherwise stated.

2.6 CELL VIABILITY ASSAYS

Several measures to ensure cell viability were performed on CHO-K1 cells after SLO permeabilization. For propidium iodide (PI) assay, after permeabilization with SLO cells were incubated with 1 ug/mL for 5 minutes on ice. At the end of staining, the cells were washed with PBS 3x. PI was imaged using 561 nm excitation and 605 nm emission. A bright field image was recorded for the same region for cell counting purposes. % viability was calculated based on the number of propidium iodide stained cells over the number of cells counted in bright field.

For cell counting experiment, CHO-K1 cells were seeded on a lettered fiduciary marker coverslip. The manufacturing process for the coverslip is described in literature[1]. The CHO-K1 cells were permeabilized following the protocol mentioned above with SLO. GBP-Atto647N was delivered inside the cell without labeling any protein just to mark the cells that are permeabilized. An initial fluorescence and bright field image was recorded right after SLO

permeabilization. After 16 hours, the same regions were located with the help of lettered fiduciary marker and another bright field and fluorescence image of the region was recorded. The number of cells present in this region was counted.

For p65 translocation assay, HeLa cell was transiently transfected with p65-Halotag, or p65-GFP. 48 hours post-transfection, the cell was permeabilized with SLO, and HeLa p65 Halotag and p65 GFP were loaded with chloroalkane-Alexa660 and GBP-Atto647N respectively. After the cell recover from SLO permeabilization, the cells were serum starved in DMEM for 4 hours prior to TNF-alpha (10 ng/mL) and Leptomycin B (LMB, 2 uM) treatment. A fluorescence image of the GFP and Atto647N channel was recorded 15 minutes and 30 minutes after the drug treatments.

2.7 KINESIN TRACKING ANALYSIS

U2OS cells were transiently transfected with plasmid DNA encoding 2xmCherry K560 (A gift from Kristin Verhey, U Michigan) for 2.5-4 hours. Post-transfection the cells were permeabilized with SLO as described above. The cells were then labeled with red fluorescent protein binding nanobody (RBP-Atto647N, Chromotek). For each cell, a 300 frames movie was recorded using 200 ms exposure time. The movie was analyzed by cropping single molecule spots that shows processive linear motion. Each frame of the cropped movies are then fitted with a 2D Gaussian function to localize the center of the molecule. The position of the molecule per frames are rotate to linearize the trajectory so that the molecule only moves in 1 dimension (x). The velocity and run length is then determined from the x position as a function of time.

2.8 LIVE CELL dSTORM AND ANALYSIS USING LIVEPALM

U2OS cells were permeabilized using the protocol mentioned above. 330 nM of Alexa647-phalloidin, or Atto488-phalloidin were loaded after permeabilization. The cells were recovered in recovery media mentioned above plus 4 mM final concentration of glutathione. After the cell recovered from SLO permeabilization, 100 uL of Oxyrase stock solution (Oxyrace, Inc.) and 20 mM final concentration of sodium DL-lactate (Sigma) were added to the cell media. Series of images were recorded after the addition of Oxyrace up to a total of 2 hours. The activation laser was 405 nm at 5-50% power, and Alexa647 was de-activated by shining 640 nm laser at 100% laser power. For experiments using Atto488, the dye was de-activated by using 488 nm laser. For static dSTORM image, a section of the cell was imaged at 20 ms exposure for 40,000 frames. For dynamic dSTORM movie 20,000 frames were recorded per cell at 100 ms exposure time per frame. For the analysis of dSTORM data, a custom software was used (LivePALM). The detail algorithm of how the single molecule detection works is published previously [2]. We've also extend the measurement to labeled mitochondria, and the protocol is mentioned above same as where we labeled the mitochondria protein ActA with Alexa660.

2.9 REFERENCES

1. Lee, S. H. *et al.* Using fixed fiduciary markers for stage drift correction. *Opt. Express* **20,** 12177–12183 (2012).
2. Li, Y., Ishitsuka, Y., Hedde, P. N. & Nienhaus, G. U. Fast and Efficient Molecule Detection in Localization-Based Super-Resolution Microscopy by Parallel Adaptive Histogram Equalization. *ACS Nano* **7,** 5207–5214 (2013).

Chapter 3

Results

3.1 SPECIFIC LABELING OF INTRACELLULAR PROTEIN IN LIVE MAMMALIAN CELLS

A general schematic of SLO permeabilization and delivery process is very straightforward and shown in Fig. 3.1. The cells are exposed to SLO toxin for permeabilization, which is followed by incubation with the probes. The external free probes are then washed away after 5 minutes of short incubation. To recover the cell, completely medium without antibiotics supplemented with ATP, GTP, and glucose, are added to the cell. The cells are then allowed to recover in the incubator for 15-20 minutes.

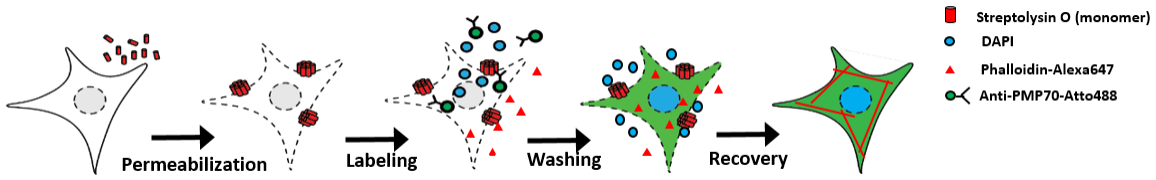

Figure 3.1. Schematic of permeabilization, delivery, and recovery steps. Cells are exposed to Streptolysin O for 7-10 minutes before incubating with the three different fluorescent probes (DAPI, phalloidin-Alexa647, and Anti-PMP70-Atto488) on ice for 5 minutes. Recovery was initiated by adding 10% FBS DMEM supplemented with nucleotide triphosphates and glucose.

To demonstrate the specific labeling of intracellular structures in untransfected cells, we simultaneously delivered three different membrane impermeant fluorescent probes (DAPI, < 1 kDa; Alexa647-Phalloidin, ~2 kDa; Anti-PMP70-Atto488, 150 kDa) into native and live CHO-K1 cells that have been permeabilized with SLO (Fig. 3.2). High permeabilization efficiency (~90%) was achieved within 10 min. Fluorescence images of SLO treated cells (Fig. 3.2, top row) revealed the stained nucleus, punctate structure of peroxisomes, and filamentous structure

of the actin – a stark contrast to SLO untreated negative control cells (Fig. 3.2, bottom row). To confirm the membrane integrity, the same set of cells were incubated with a fluorescent marker molecule (Texas Red dextran, 20 kDa) after 20 min of recovery time. Membrane of recovered cells efficiently excluded Texas Red dextran (Fig. 3.2 top right). The negative control cells also showed no fluorescence signal until cells were permeabilized by SLO (Fig. 3.2 bottom row right). Through further viability tests after the recovery step, we found that close to 95% of cells had intact membrane (Fig. 3.3), and showed proper cell division (Fig. 3.4). In addition, we performed p65 translocation assay on human cancer cell line (HeLa), where the cells were permeabilized, and intracellular p65-GFP or p65-Halotag was labeled with GBP or Halotag Ligand. We observed translocation of labeled p65 into the nucleus upon treatment with TNF-alpha (Fig. 3.5). The strength of the response is comparable to that of cells untreated by SLO (blue circle), which is about a 70% increase in fluorescence intensity inside the nucleus. Furthermore, with the addition of Leptomycin B (LMB), a nucleus export inhibitor, we saw an accumulation of p65 inside the nucleus at a level higher (~200%) than TNF-alpha alone. This is a proper response of the p65 to a nucleus export inhibitor, where the p65 are unable to be recycled back to the cytoplasm. This technique can potentially be applied to perform similar assay on native cells. For instance, antibody probes can be delivered using SLO permeabilization to label proteins that are relevant to cancer cell metabolism. We can then monitor the activity of labeled native proteins in response to various molecules for drug screening.

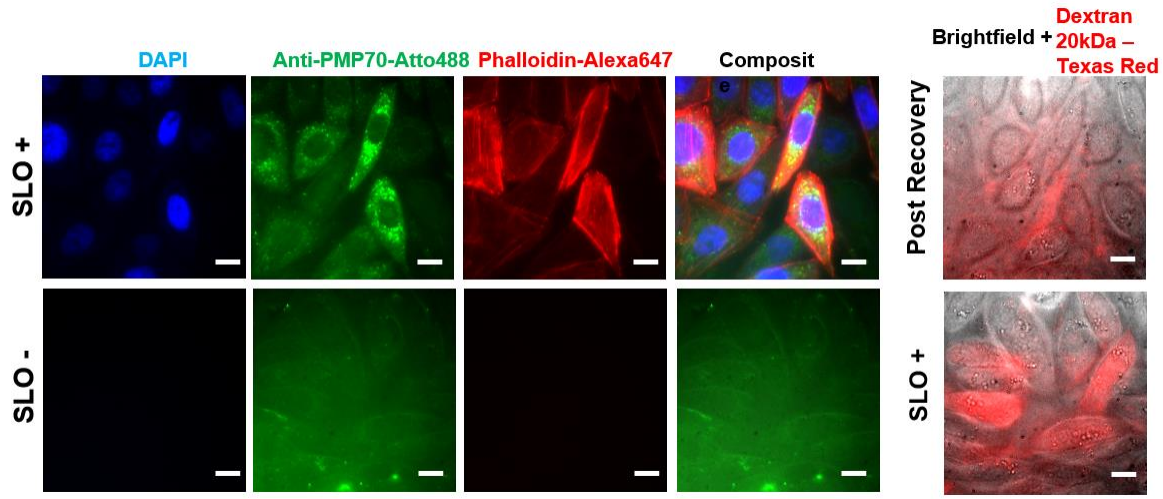

Figure 3.2. Specific labeling of cellular structures by SLO delivered probes. Nucleus, peroxisome, and actin filaments are labeled by DAPI, Anti-PMP70-Atto488, and phalloidin-Alexa647 respectively. The cells are then incubated with Texas red- 20 kDa dextran to check whether the membrane has recovered. The negative control (SLO-) shows no labeling of cellular structure. The negative control cells are then permeabilized by SLO to show the fluorescence of Texas red in permeabilized cells. (With CHO cells, as opposed to other mammalian-type of cells, DAPI is cell impermeant.)

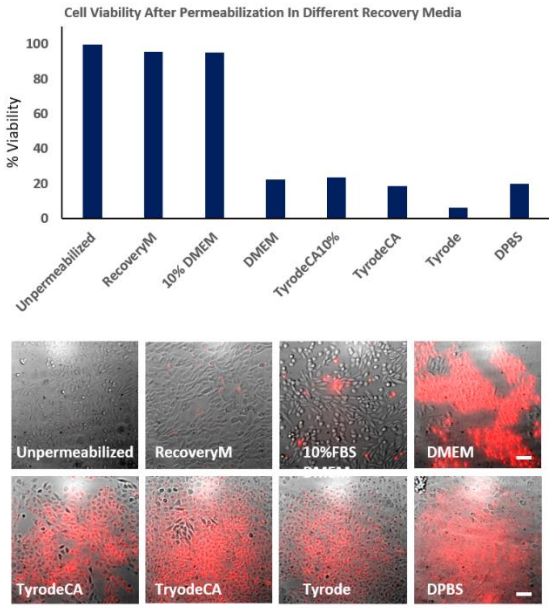

Figure 3.3. Propidium iodide assay performed on CHO-K1 cell after SLO permeabilization and recovery. The CHO-K1 cells were recovered in different buffers after permeabilization. Only recovery media and 10% FBS DMEM successfully excluded the cells from PI staining. Scale bar denotes 50 μm.

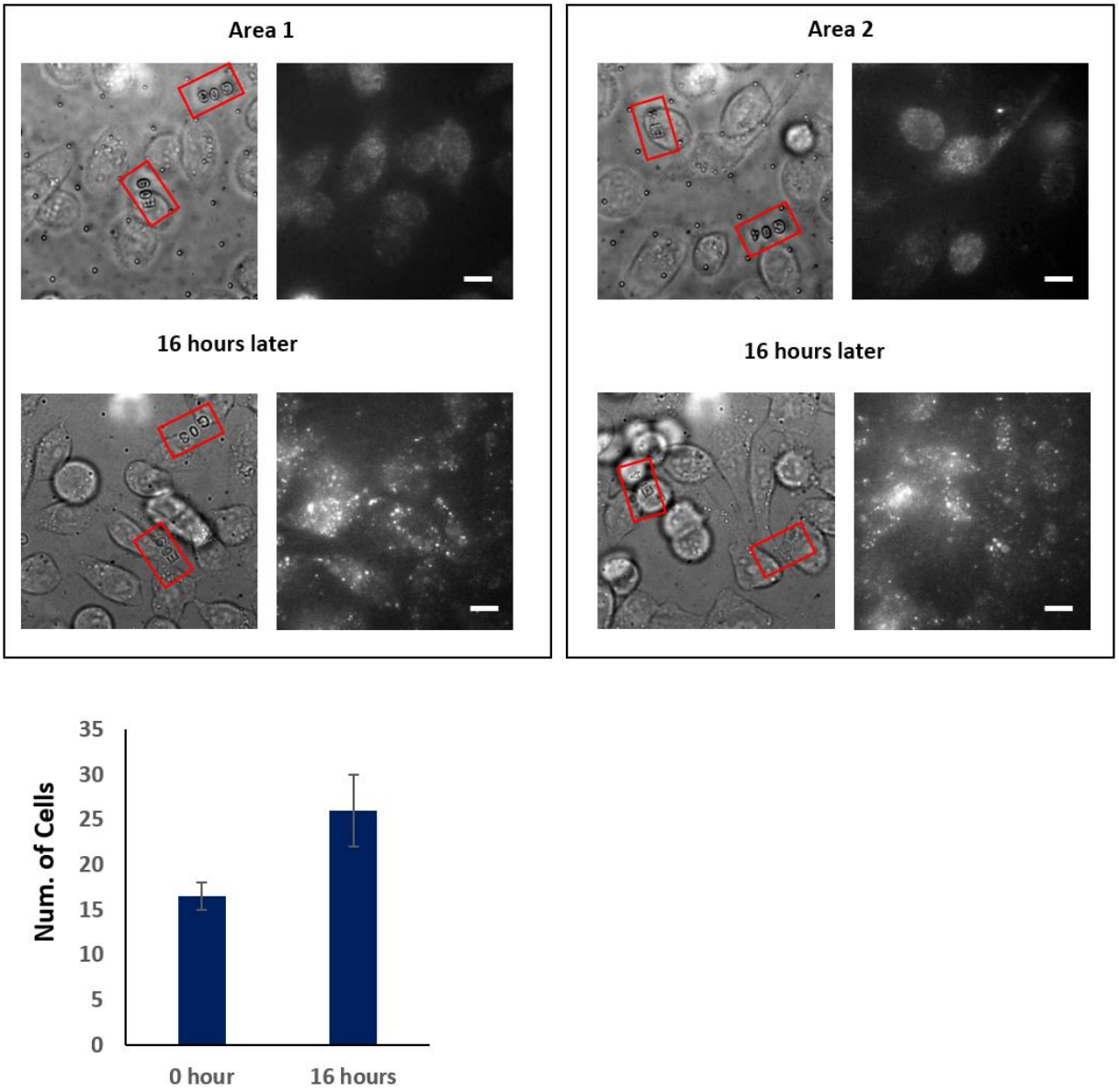

Figure 3.4. CHO-K1 cells cultured on lettered fiduciary marker for 16 hours after delivering GBP-Atto647N probes. The number of cells are counted in the region initially and after 16 hours. The number of cells increased by nearly 60% despite SLO treatment, suggesting cells were able to undergo cell division. Scale bar denotes 10 μm.

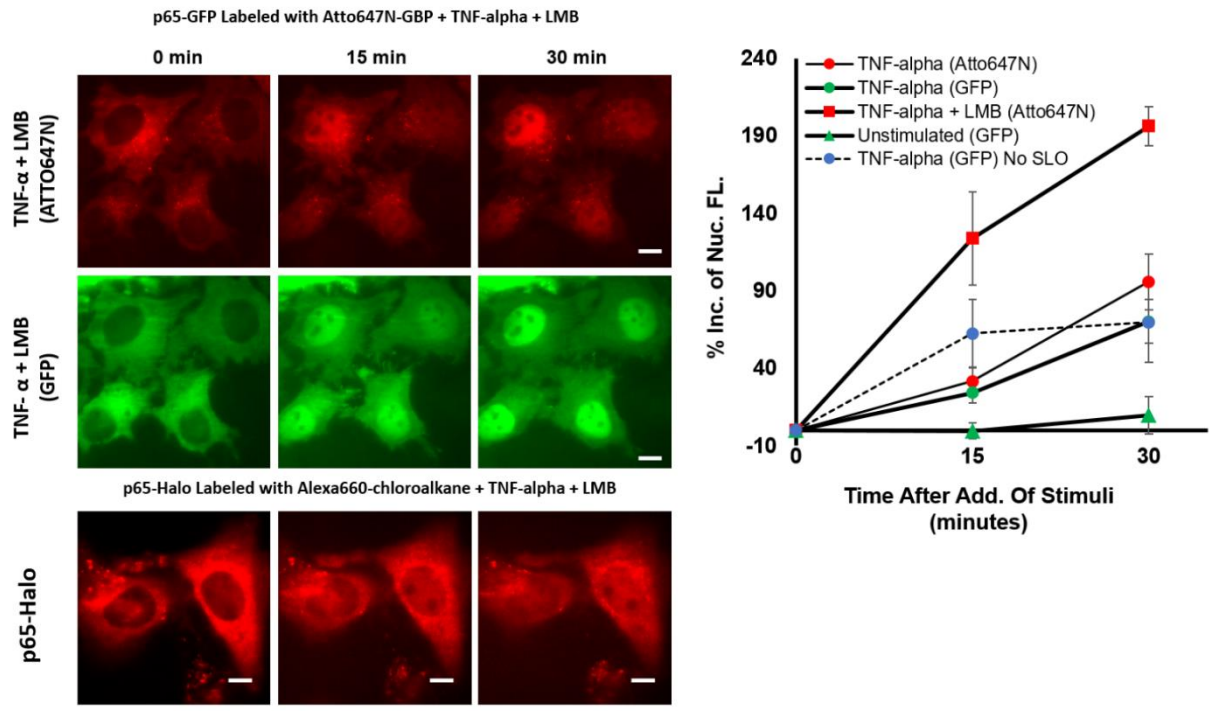

Figure 3.5. Observing Live cell dynamic using p65 Translocation Assay after SLO permeabilization. TNF-alpha and Leptomycin B were used to stimulate nucleus import of the p65-GFP protein labeled by GBP-Atto647N. The Nucleus fluorescence of both GFP and Atto647N channels increased 15 and 30 minutes after stimulation, suggesting TNF-alpha stimulated IKB removal to bring the p65-GFP into the nucleus. (Red square= Atto647N intensity in the nuclear after TNF-alpha and LMB treatment, Green circle = GFP intensity after TNF-alpha treatment [N=4 cells], Red circle =Atto647N Intensity after TNF-alpha treatment [N=4 cells]. Blue circle with dashed line is GFP intensity after TNF-alpha treatment for cells never been permeabilized by SLO [N=4 cells]. Green triangle = GFP intensity without TNF alpha and LMB treatments [N=3 cells].) An example of p65-halotag is also given, labeled with Alexa660 chloroalkane.

3.2 SPECIFIC LABELING OF INTRACELLULAR PROTEIN IN TRANSFECTED MAMMALIAN CELLS USING A VAIRETY OF PROBES

Furthermore, our technique can be extended to label any intracellular proteins by using transfected cells, where additional tag such as Halotag or GFP are fused to the protein of interest.

Here, we have transfected cells with GFP-ActA-Halotag, a protein that binds to the mitochondrial membrane, and our goal is to label this particular protein using different probes so that the structure of mitochondria is fluorescent. The probes either target the mitochondrial membrane protein through immunolabeling of GFP or through ligand binding action of Halotag. Specific labeling is demonstrated by comparing the fluorescence image of the probes to the image of GFP channel (Fig 3.7). Through SLO permeabilization, all of the probes tested (chloroalkane-Alexa660, GBP-Atto647N, Chloroalkane-Biotin-Streptavidin-Atto647N, Anti-GFP IgG) were able to specifically label the mitochondria. However, these probes are different in size, and one has to consider under what scenario each of these probe would be used.

One consideration for the size of the probe being delivered is whether it makes it across the nucleus. We demonstrated this by labeling GFP fused Proliferating Cell Nuclear Antigen (GFP-PCNA) using GBP-Atto647N (Fig. 3.7). We found that single domain nanobody, in this case specific to GFP (GBP), makes it across the nucleus and were able to label nuclear protein, whereas probes larger than GBP, such as streptavidin (SA) were not able to passively diffuse across the membrane. We have also delivered fluorescein– dextran to confirm this fact that 70 kDa dextran which is comparable to the size of SA is not able to make it across the nucleus membrane (Fig. 3.6), but 40 kDa dextran did make it across and its fluorescence is diffused across the cell homogenously.

Surprisingly, we discovered that probes larger than dye conjugated ligand shows retention inside the cells after recovery, which appears as homogenous background fluorescence across the cytosol. This makes the size of the probes delivered using SLO permeabilization an important factor to consider for different experiment, because different sizes of probes has different advantages for labeling intracellular proteins (Fig. 3.7). One significant advantage of

using pore-forming toxin for probe delivery over other methods, such as microinjection, is that unlabeled free probes can be washed away. Small probes and small molecules, such as conjugated phalloidin, chloroalkane (for Halotag), leaks out by the end of washing and resealing (Fig. 3.6.). Consequently, essentially background-free signal is achieved.

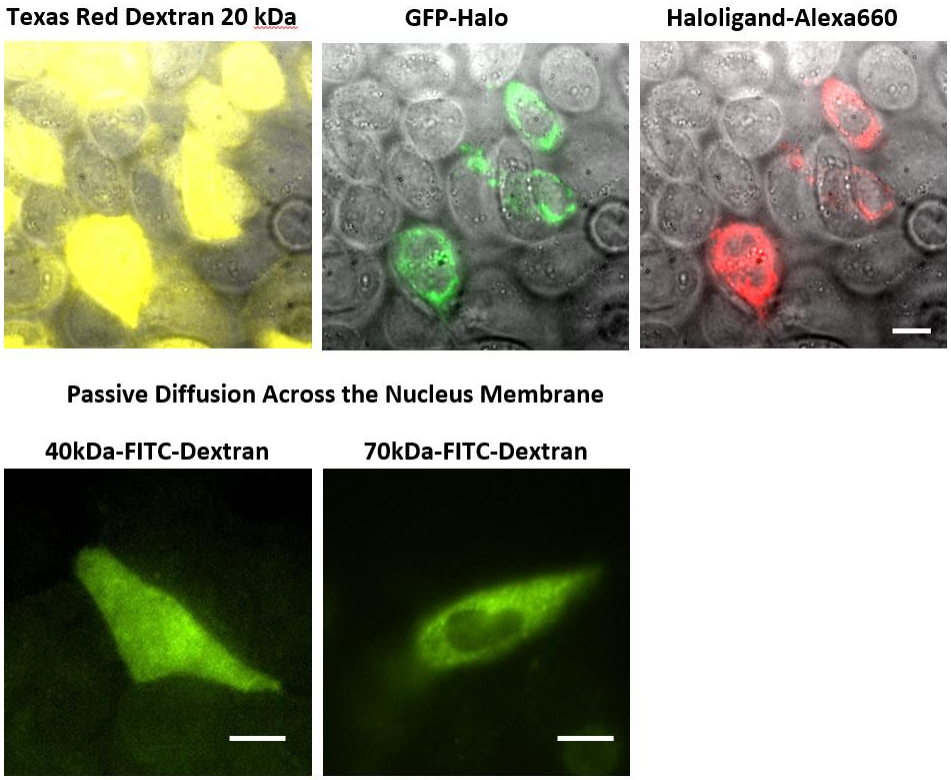

Figure 3.6. The effect of ligand size on probe retention and nucleus permeability. The Texas Red Dextran image (yellow) shows all of the cells that were permeabilized, which a haze of fluorescence across the whole cell, whereas the chloroalkane-Alexa660 being <2 kD only stains the cells expressing the GFP-halo protein; no homogenous red fluorescence was observe in other permeabilized cells. Free chloroalkane-Alexa660 were washed out during our procedure. In terms of nucleus accessibility, we tested the mw-cutoff with fluorescein dextran on CHO-K1 cells. We observed homogenous fluorescein fluorescence using 40 kDa-dextran, whereas 70 kDa-dextran the fluorescence was excluded in the nucleus. Scale bar denotes 10 μm.

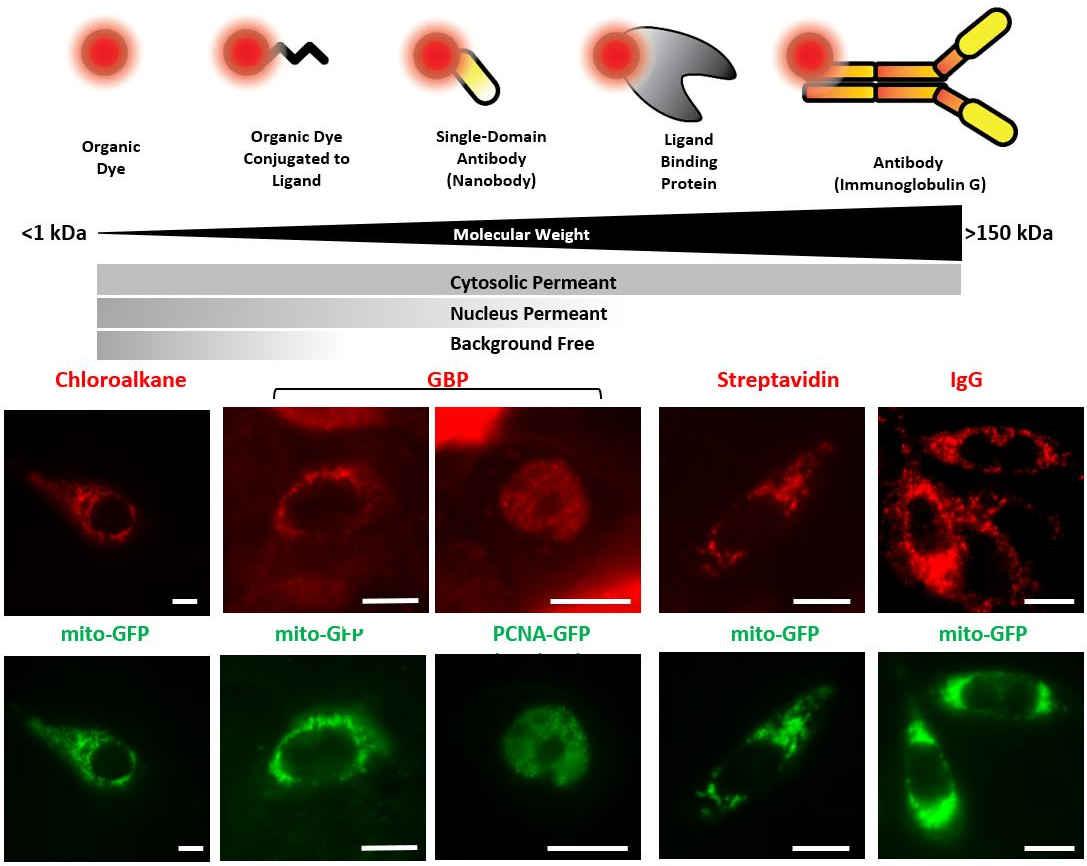

Figure 3.7. Delivery of different sized fluorescent probes for specific labeling of intracellular protein. Delivery of different sized fluorescent probes for specific labeling of intracellular protein. Cells that are labeled by various SLO delivered probes are shown (top row) to compare with their intracellular or nucleus target, which is tagged with GFP (bottom row). All the probes loaded, up to 150 kDa IgG were successfully delivered by SLO and labeled target proteins. However, only small proteins such as GBP (14 kDa) was able to access the nucleus target. Small ligands with roughly 2 kDa molecular weight can be washed away, which only leaves the transfected cells labeled. Scale bar denotes 10 μm.

3.3 KINESIN TRACKING USING DELIVERED NANOBODY PROBES

We have also utilized SLO permeabilization for delivering fluorescent probes that are much more photostable than FP for single particle tracking. As an example of this, we tracked single kinesin molecules in the cytoplasm of U2OS cells. We transfected the cells with 2x-mCherry Kinesin 560, a truncated version of dimeric kinesin-1. Based on the fluorescence of

mCherry alone, it is extremely hard to track a single kinesin protein, due to poor signal to noise ratio and over-expression of the protein. Previously, attempt has been made to over-come this by expressing a 3x tandem FP kinesin construct[1]. However, it was found that the truncated version of kinesin fusion protein is not motile. Here, we enhance the signal by delivering RFP binding nanobody (RBP-Atto647N). A single kinesin can bind up to four RBP-Atto647N for enhanced photon output (Fig. 3.8).

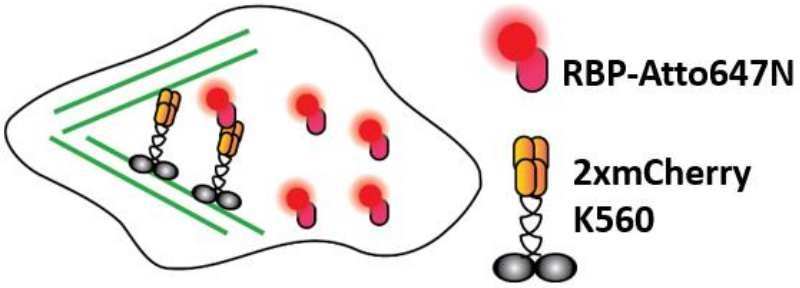

Figure 3.8. Tracking nanobody labeled single kinesins in live U2OS cells.

Each RBP has a single binding domain for mCherry. Therefore, the stoichiometry is favorable for detecting a single kinesin protein. To demonstrate the specificity of the nanobody probe (RBP-Atto647N). We first tried recovering the cells in the absence of ATP. The results are shown in Fig 3.9. We saw a majority of kinesin accumulating on the microtubule. This is to be expected in a condition where ATP is very scarce. The specificity of the probe is demonstrate by overlapping the mCherry fluorescence image with the Atto647N image. We observed colocalization of the two channels, which indicated to us that the probe is very specific. Next, we went on to recover cells under saturating ATP condition, and we also purposely under label the kinesin so that minimum freely diffusive probe was observed. In Fig. 3.10. we observed the fluorescence image of mCherry accumulating at the tip of the cell, which is an indication that ATP in the cell is abundant. Because of the over-expression of the kinesin protein, it is very hard

to track individual molecular motor. We then photobleached the FPs so that it is easier to see individual molecules. However, due to the poor S/N, it was still difficult to track kinesin using FP under this condition. Once we labeled the kinesin with Atto647N, the kinesins becomes much easier to track, and individual spots can be easily tracked in the whole cell. As demonstrated by the overall trajectory of molecules detected, most of the traces are around a micron, which agrees with the run length of kinesin (Fig. 3.11). The velocity of individual kinesins were tracked and a histogram was compiled from the velocities (Fig. 3.12). We observe that the velocity of kinesins in cells was 1058 ± 22 nm/s (Center ± S.E.M.) at 30 °C. At room temperature (22 °C), the velocity of kinesin lowered to 541 ± 16 nm/s (Center ± S.E.M.). The effect of temperature on the enzymatic activity of kinesin and resulting velocity was previously studied *in vitro*[2,3]. Our results suggest that kinesin's velocity is heavily influenced by temperature of the cell, and not just *in vitro*. Overall, we showed that at the single protein level, velocity of truncated kinesin is almost identical *in vitro* and *in vivo*.

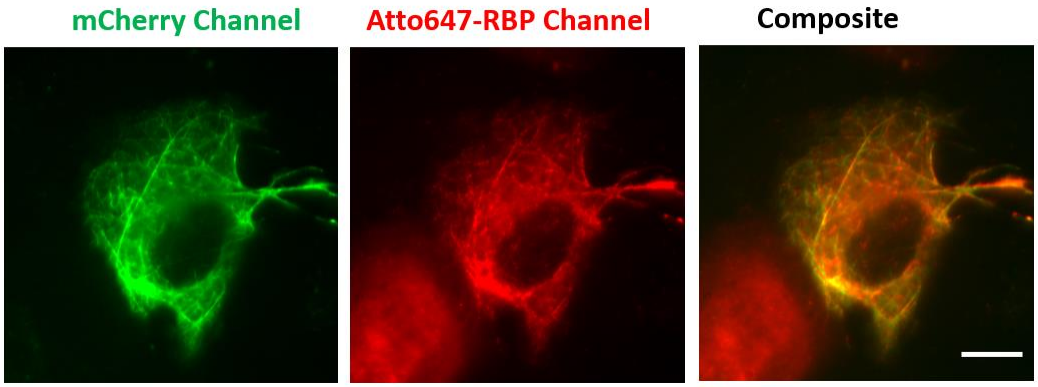

Figure 3.9. Labeling of mCherry Kinesin without ATP Supplement. mCherry kinesins are shown to accumulate on the microtubule (green). Atto647N-RBP fluorescence is shown in red. Specific labeling is demonstrated by the overlap of two fluorescence images (yellow).

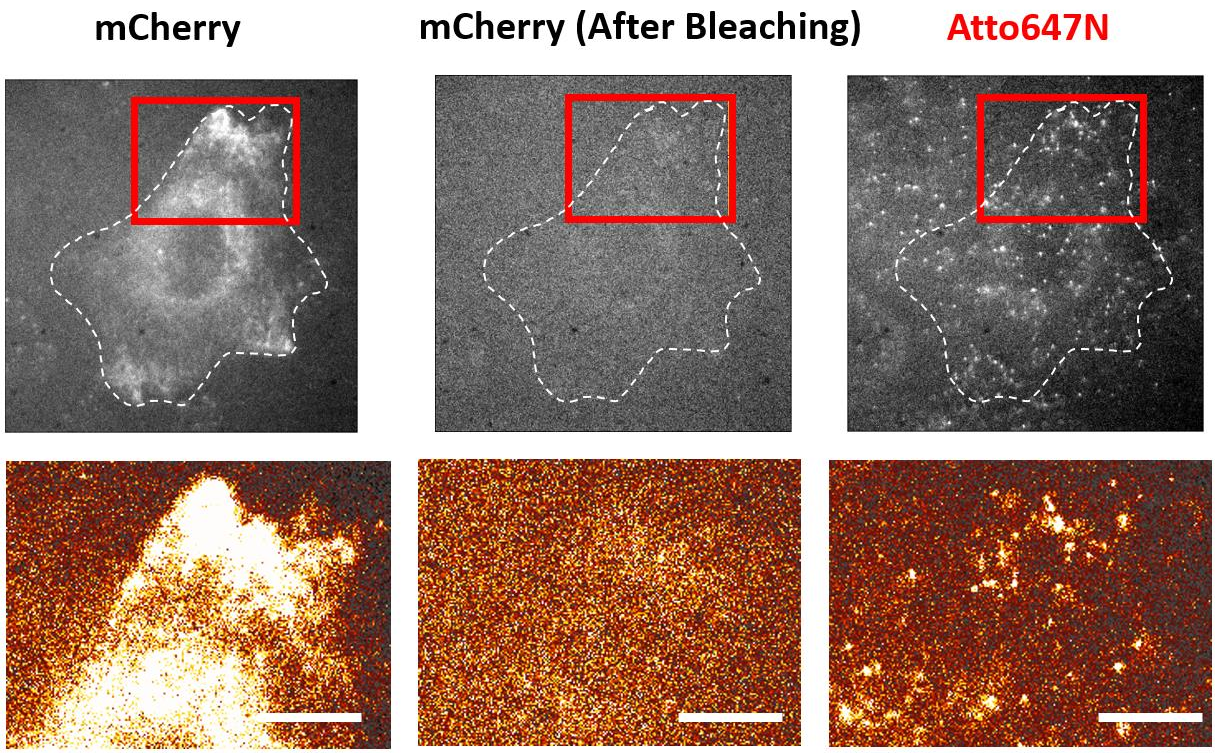

Figure 3.10. Expression and Labeling of mCherry Kinesin in U2OS cells. After just 3 hours of expression, the cell is filled with over-expressed mCherry kinesin, and it isn't possible to track individual protein. Single kinesin molecules can easily be tracked by sparsely labeled mCherry kinesin with Red fluorescent protein binding protein (RBP) conjugated to Atto647N. Scale bar denotes 10 μm.

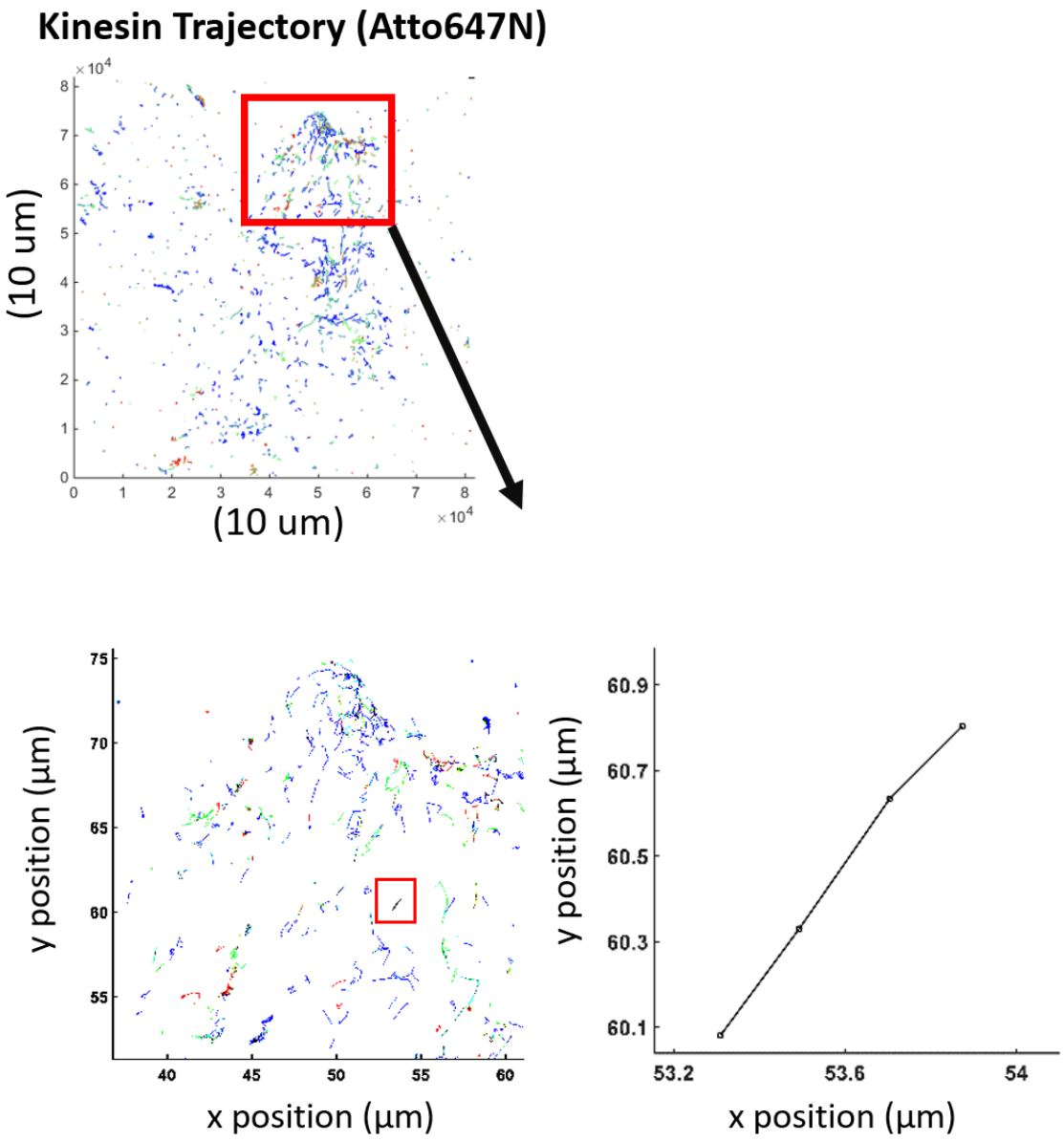

Figure 3.11. Tracking individual Atto647N-RBP labeled kinesin. Majority of kinesin trajectory in the selected area can be seen to travel uni-directionally in a short distance (<5 micron). The trajectory enclosed in the red rectangle is an example trace of detected kinesin trajectory.

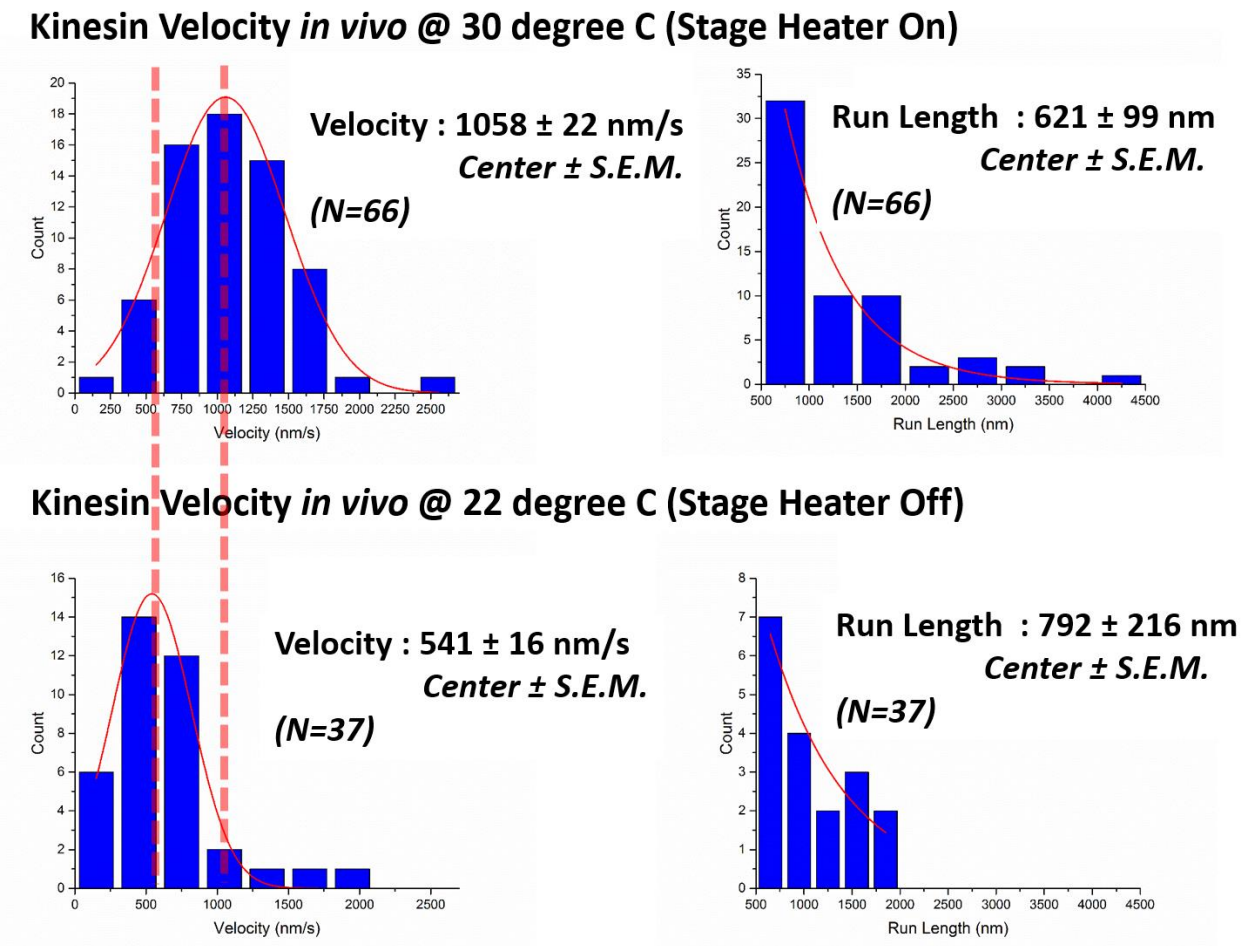

Figure 3.12. Quantitative Analysis of Labeled Kinesins. To quantify the kinesin behavior in vivo, velocity and run length of labeled kinesin were measured. The kinesins are moving at an average velocity of 1058 ± 22 nm/s (Center ± S.E.M.), and the average run length is 621 ± 99 nm (Avg ± S.E.M.). The measurements were taken on a heated stage at 30 degree Celsius. At 20 degree Celsius, Gaussian fitting shows a velocity of 541 ± 16 nm/s (Center ± S.E.M.). Average run length is found to be 792 ± 216 nm (Center ± S.E.M).

3.4 dSTORM IN LIVE CELL USING SLO DELIVERED CELL IMPERMEANT PROBES

We demonstrate the ability to observe live cell dynamics in both macro and microscopic scale by looking at the dynamic of actin in live cell, labeled with cell impermeant probes through direct Stochastic Optical Reconstruction Microscopy (dSTORM) [4]. Currently, there are a limited number of commercially available cell permeant ligands and fluorophores for dSTORM. For

instance, popular dSTORM fluorophores for *in vitro* imaging, such as Cy3B and Alexa647 are cell impermeant. Attempt to overcome this limitation was made by injecting the fluorescent probes using microinjection method[5]. The advantage of our method however, is that small unlabeled probes exit the cell during washing and recovery, so minimum background is achieved.

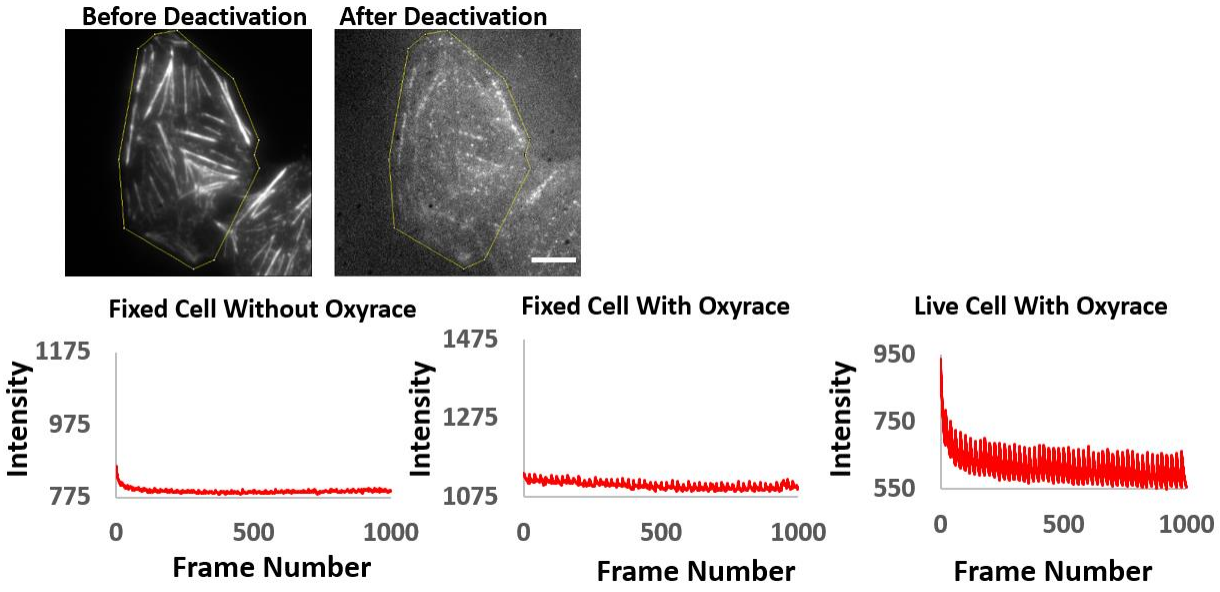

Figure 3.13. Activation of Alexa647 on actin in fixed cells and in live cells in the presence of Oxyrace. U2OS cells with actin staining are deactivated by high power illumination using 640 nm laser (Top row). Scale bar denotes 10 μm. Pulses of 405 nm lasers are applied to the either fixed or live cells with stained actin, and the intensity as a function of frame number is plotted. If the probe reactivated, spikes of intensity increase would be observed. No reactivation was observed without addition of Oxyrace on fixed cell. Even with addition of Oxyrace alone, there was very little activation in fixed cell. The environment of living cell combined with Oxyrace make reactivation possible. Scale bar denotes 10 μm.

In order for dSTORM to work on live cell, two criteria has to be satisfied; an oxygen scavenging system that works intracellularly, and presence of thiol containing reducing agent. To keep the oxygen concentration low, we utilized live cell compatible oxygen scavenging system

called Oxyrace, where we observed almost no reactivation of Alexa647 without Oxyrace (Fig. 3.13). The cells natively contain reducing agent, such as glutathione, and has been reported to work for the acquisition of dSTORM images using fluorophore (Atto655) dSTORM [6]. In fixed cell where no reducing agent was present, the activation was poor, even with oxygen scavenger present. To make dSTORM work with the SLO technique, we had to supplement glutathione in the recovery media. It was previously discovered that small molecules, such as ATP, may escape the cell during severe SLO permeabilization [7]. After we supplemented our recovery media with glutathione, indeed we observed higher activation events from Alexa647, and lower background, meaning the fluorophore is being more effectively turned off (Fig 3.14).

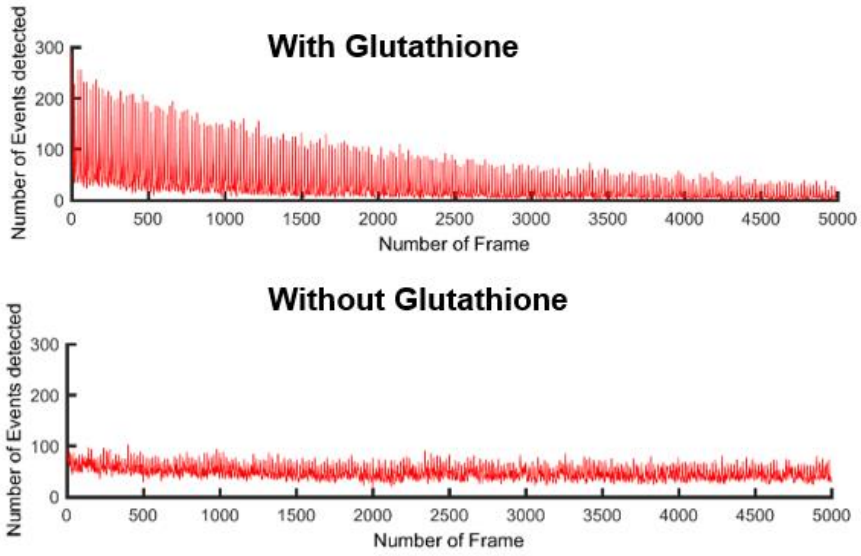

Figure 3.14. Number of detected activation events per frame with and without the addition of glutathione in the recovery media. With the addition of 4 mM of glutathione in the recovery media after SLO permeabilization, there are more number of activation events detected per frame, as well as less number of detected events during illumination, suggesting that the added glutathione assists in turning off the fluorophore more efficiently

Here, we delivered a cell impermeant fluorescent probe (Alexa647-Phalloidin) to specifically label actin filaments in living cell. A region of the U2OS cell with labeled actin are shown in conventional fluorescence image and super-resolution d-STORM image. The image was collected at 20 ms time resolution for a total of 40,000 frames (Fig 3.15). We further demonstrate the capability of observing long time dynamics, where with the addition of Oxyrace/Glutathion we observed actin dynamics extending over the long-time of > 30 minutes. In a longer movie that we acquired with 100 ms per frame for a total of 20,000 frames. We observed a thick actin bundle split into two over the course of ~3 minutes (Fig. 3.16).

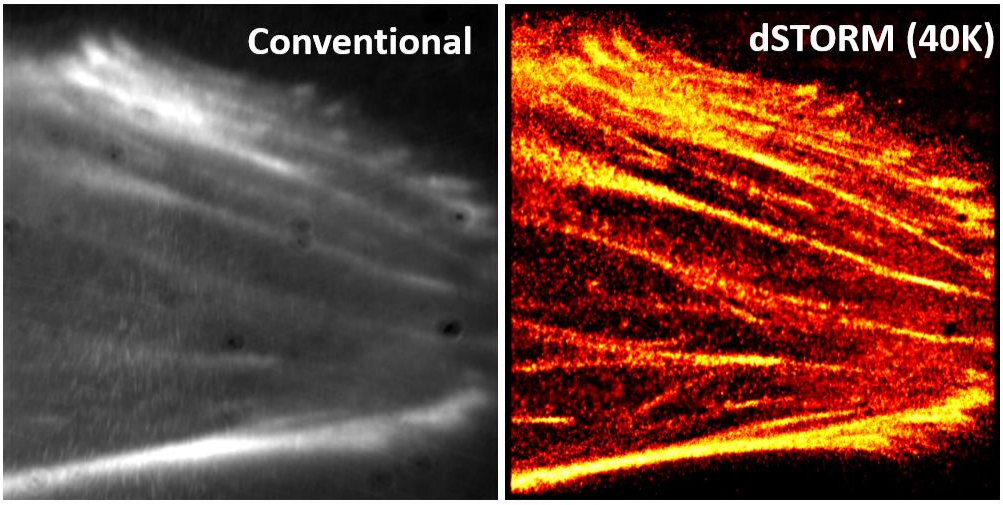

Figure 3.15. Comparison of conventional FL image vs dSTORM image. Phalloidin-Alexa647 was delivered via SLO permeabilization. A region of densely packed actins that are hard to resolve is shown in the conventional fluorescence image. A dSTORM image is reconstructed from the same section of the cell, which resolves the actins much better. The dSTORM image was reconstructed from 40,000 frames of activation and deactivation events, each frame was taken at 20 ms exposure time for a total of 13 minute 20 seconds of acquisition time.

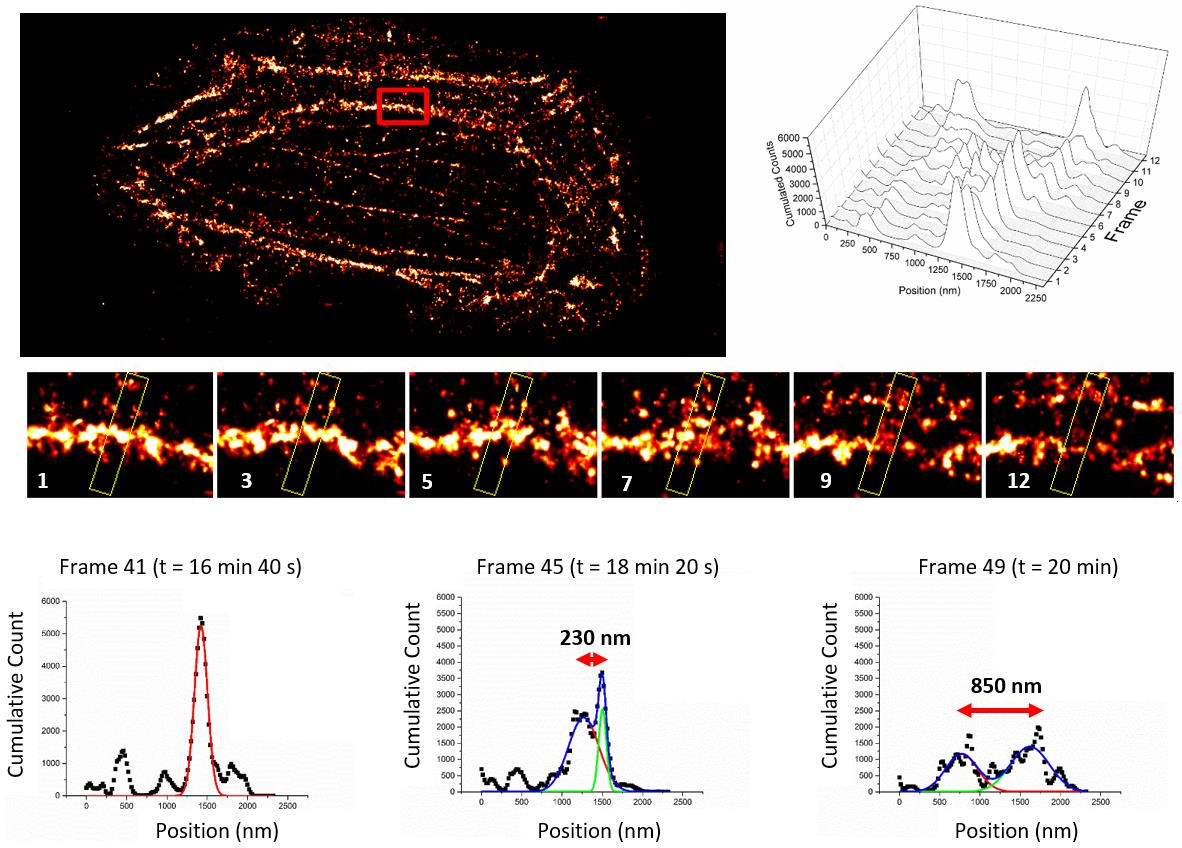

Figure 3.16. A dynamic dSTORM movie was acquired to examine large scale actin dynamics. Each frame of the movie is composed of 500 frames, with a 250 frames moving average time window. The movie was recorded for a total of 20,000 frames at 100 ms exposure time, for a total acquisition time of over 30 minutes. Focusing on a small section of the image, a thick actin bundle can be seem to split into two smaller actin filaments. The actin filaments grew 230 nm apart after 1 minute 40 seconds, and then 850 nm apart after another 1 minute 40 seconds.

We've also extended this measurement on a different wavelength dye, and a different cytosolic target. We tried using Atto488-Phalloidin instead of Alexa647-Phalloidin, since Atto488 is also listed as one of the dSTORM dyes. We noticed that Atto488 is less reactive towards 405 nm, that is, the fluorophore does not "turn on" in response to 405 nm illumination. However, Atto488 blinks a lot, and using blinking to detect individual fluorophores we were able to construct a super-resolution image (Fig. 3.17). A comparison between convention and super-resolution shows clearly the actin filaments. The number of blinking event detected using

Atto488 was roughly 50 per frame, which makes it less efficient for dSTORM than Alexa647, where more than 100 activation events were detected per frame.

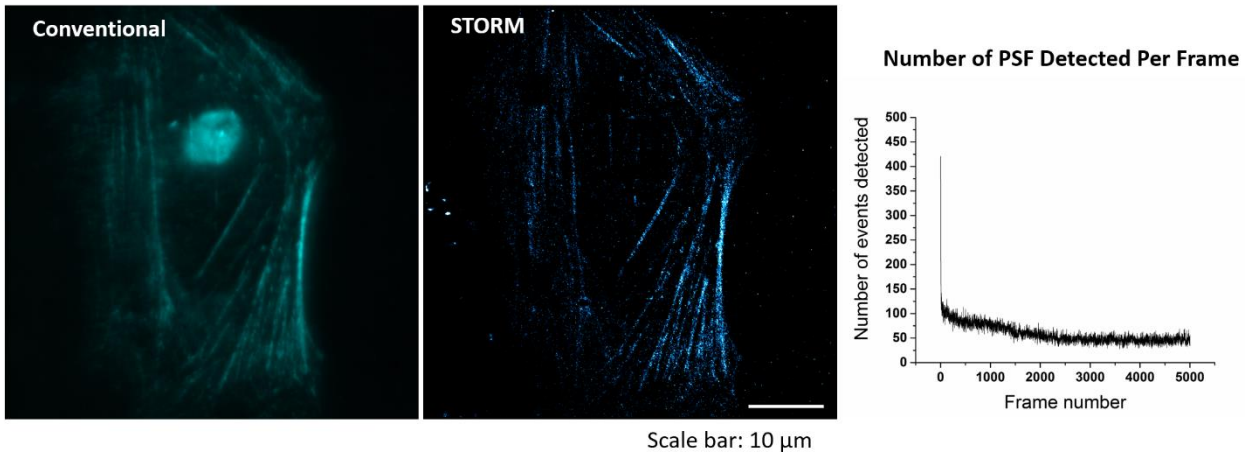

Figure 3.17. Super-Resolution image of actin using Atto488-Phalloidin.

Next, we tried to label a different cytosolic target other than actin, and we decided to label the mitochondria via Halotag using previously describe protocol. The difference is that Oxyrace and Glutathione are now added in order to cause reactivation and prolonged photostability. The fluorophore used for labeling was Alexa660. The dye claimed to be used for super-resolution imaging in one paper[8], our experience when using it for conventional imaging was that it shows extremely poor photostability. Nonetheless, we were able to record super-resolution image of mitochondria using this dye (Fig. 3.18). Because of the fact that the labeled ActA protein diffuses along the mitochondrial membrane, it was able to fill out the shape of mitochondria very well by single particle tracking dSTORM (SPT-dSTORM)[9]. In Fig. 3.18A a conventional image and SPT-dSTORM image of the mitochondria in U2OS cells are shown. There are a lot more mitochondria in conventional image, due to the fact that the mitochondria is very dense in cells, and it was not possible to de-activate all of the out of plane mitochondria given the depth of the cell. The improvement of super-resolution image can be seen by looking at

a particular mitochondria that appeared to be circular (Fig. 3.18B). The circular shape of the mitochondria appear to be a filled sphere in conventional image, however, SPT-dSTORM image reveals that it is actually hollow. Not only was SPT-dSTORM an improvement of the spatial resolution, we were able to observe dynamic using this technique as well. Fig. 3.18C shows the dynamic of spherical mitochondria over the course of ~5 minutes. The mitochondria traveled roughly 1.5 microns in the course of 5 minutes. It showed an initial backward motion in the first 2 minutes, then migrate towards the opposite side for the next 3 minutes.

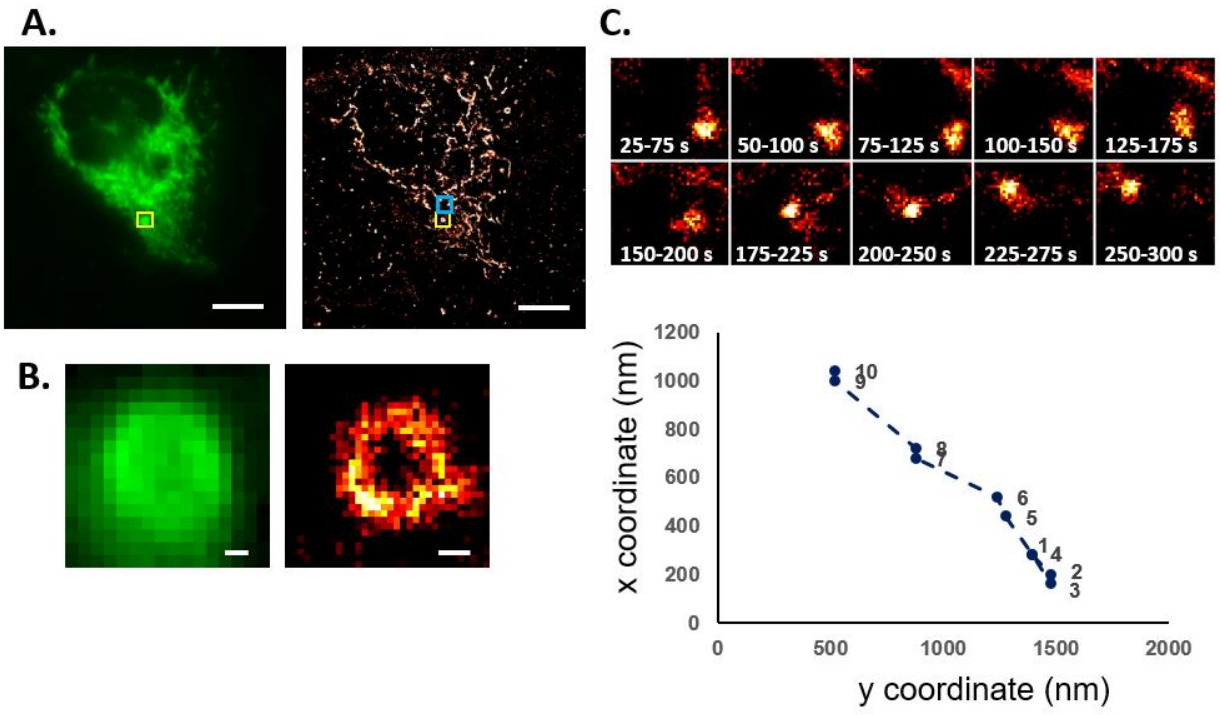

Figure 3.18. SPT-dSTORM Image of Mitochondria in Live U2OS cells. A) Conventional image of GFP-mitochondria (left), and SPT-dSTORM image of mitochondria (right). The area enclosed in yellow and blue squares are further analyzed in sub-figure B and C. Scale bar denotes 10 μm. B) Conventional image of a circular mitochondria (left), and SPT-dSTORM image of mitochondria (right). Scale bar denotes 200 nm. C) Mitochondria dynamic in U2OS cell is observed over the course of 275 seconds. The trajectory of the mitochondria is shown (bottom).

3.5 REFERENCES

1. Tracking Single Kinesin Molecules in the Cytoplasm of Mammalian Cells. Available at: http://www.sciencedirect.com/science/article/pii/S000634950771216X. (Accessed: 9th May 2016)
2. Böhm, K. J., Stracke, R., Baum, M., Zieren, M. & Unger, E. Effect of temperature on kinesin-driven microtubule gliding and kinesin ATPase activity. *FEBS Lett.* **466,** 59–62 (2000).
3. Kawaguchi, K. & Ishiwata, S. 'ichi. Temperature Dependence of Force, Velocity, and Processivity of Single Kinesin Molecules. *Biochem. Biophys. Res. Commun.* **272,** 895–899 (2000).
4. Heilemann, M. *et al.* Subdiffraction-Resolution Fluorescence Imaging with Conventional Fluorescent Probes. *Angew. Chem. Int. Ed.* **47,** 6172–6176 (2008).
5. Hennig, S. *et al.* Instant Live-Cell Super-Resolution Imaging of Cellular Structures by Nanoinjection of Fluorescent Probes. *Nano Lett.* **15,** 1374–1381 (2015).
6. Wombacher, R. *et al.* Live-cell super-resolution imaging with trimethoprim conjugates. *Nat. Methods* **7,** 717–719 (2010).
7. Walev, I. *et al.* Delivery of proteins into living cells by reversible membrane permeabilization with streptolysin-O. *Proc. Natl. Acad. Sci. U. S. A.* **98,** 3185–3190 (2001).
8. Żurek-Biesiada, D. *et al.* Quantitative super-resolution localization microscopy of DNA in situ using Vybrant® DyeCycle™ Violet fluorescent probe. *Data Brief* **7,** 157–171 (2016).
9. Biermann, B. *et al.* Imaging of molecular surface dynamics in brain slices using single-particle tracking. *Nat. Commun.* **5,** 3024 (2014).

Chapter 4

Conclusion

4.1 SLO PERMEABILIZATION AS A TECHNIQUE TO INTRODUCE FLUORESCENT PROBES

Our results demonstrate the practicality of delivering fluorescent probes using reversible permeabilization by pore-forming toxin. Delivering small probes (<2 kDa) using SLO permeabilization has significant advantage in experiments where high signal to background ratio is required. Free and unbound probes are washed away during the washing steps or recovery step. Nanobody probe (14 kDa) is efficient to deliver in experiments where nucleus protein has to be labeled. Due to its single binding domain, it is particularly useful as well in single molecule tracking experiment, where 1:1 protein to probe stoichiometry is important. For experiment where the photon output is important, a larger probe such as SA, or even IgG can be used, where there are multiple fluorophores on the protein. Ultimately, the probes that can be delivered using this method is not limited to the probes used in these examples; with this technique, any fluorescent probe within the size limit can potentially be delivered inside the cell for the purpose of specific labeling of intracellular protein. The technique can be coupled with other photon enhancement method, such as "spaghetti monster", where a protein of interest is labeled by multiple probes at once for signal enhancement[1].

Furthermore, this technique makes it possible to perform live cell with various probe, and will benefit from reagents that enhances photostability of dyes in live cell. For example, reagents such as Oxyrace can be used to keep the oxygen concentration low, and further improve the photostability of the probes in cells. We also show that by supplementing the recovery media with glutathione and ATP, the SLO permeabilization technique can be tailored to suit the

specific experimental need for the biological problem of interest. The application to other non-fluorescent markers, e.g. metal markers for electron microscopy and chemicals for in vivo anti-cancer drugs, is still being tested.

4.2 TRACKING SINGLE KINESIN PROTEIN IN U2OS CELLS

We found that the velocity of truncated kinesin U2OS cells closely resemble that of *in vitro* measurements done previously by others[2]. The velocity we measured is from single kinesins, as verified by its run length. It isn't possible for this truncated kinesin to be carrying cargoes, as the kinesin has no light chain or cargo binding domain, where the scaffolds for cargoes are usually attached to. The question of how the velocity of vesicles being transported in cells can reach several microns per second still remains to be solved[3]. Based on our studies, the elevated temperature of living cell can increase the velocity of kinesin by two folds- to roughly a micron per second. Our technique serves as a useful tool to study the translocation of proteins *in vivo*. There has been on-going effort to label native kinesins, instead of the truncated ones, using antibody fragments in order to study the properties of native molecular motors.

4.3 DYNAMIC DSTORM MEASUREMENT ON LIVING CELLS

dSTORM or STORM is usually associated as a technique used to study fixed cells, due to the limitation of the fluorescent probes. Here, we have broken the barrier and enabled the use of this technique on living cells, by introducing cell impermeant dSTORM probes using SLO permeabilization. The trick to be able to perform immediate measurement after permeabilization is to supplement the recovery media with glutathione to replenish those that had leaked out. An oxygen scavenging system that is compatible with live cells was used to extend the lifetime of

fluorophore to > 30 minutes. By performing dSTORM on living cell, we were able to observe the motion of actin filaments *in vivo*. We also observed first hand, how phototoxicity can be damaging in live cell imaging, by observing the shrinking of the cell and its cytoskeleton network. This will be an on-going challenge to this kind of long-duration live cell imaging technique. We are currently exploring options to perform dSTORM on a different protein of interest, other than actin, and potentially that will introduce less phototoxicity in cells. For instance, we tried to apply dynamic dSTORM on mitochondrial membrane protein ActA. With the aid of diffusive motion of ActA, the trajectory of labeled ActA can be tracked so that less number of frames are required to obtain a complete outline of the mitochondrial membrane. Using this method we have successfully observed improvement in spatial resolution of the fluorescence image, and captured dynamic motion of the mitochondria. Success in obtaining long duration dynamic dSTORM images further demonstrate the broad applicability of our technique on various imaging applications.

4.4 REFERENCES

1. Viswanathan, S. *et al.* High-performance probes for light and electron microscopy. *Nat. Methods* **12,** 568–576 (2015).
2. Norris, S. R., Núñez, M. F. & Verhey, K. J. Influence of Fluorescent Tag on the Motility Properties of Kinesin-1 in Single-Molecule Assays. *Biophys. J.* **108,** 1133–1143 (2015).
3. Allen, R. D., Metuzals, J., Tasaki, I., Brady, S. T. & Gilbert, S. P. Fast axonal transport in squid giant axon. *Science* **218,** 1127–1129 (1982).

Chapter 5

Intramolecular, Head to Tail Distance of Kinesin-1 Measured via SHREC

5.1 BIOLOGICAL MOTIVATION

The orientation of kinesin's stalk influences the position of the cargo during cellular transport. Earlier published work indicated that the neck coiled-coil, below Hinge I, is oriented perpendicular to the long-axis of the microtubule near the microtubule surface. This helps explain the asymmetric walk of kinesin. However, these experiments were done in the absence of ATP with a truncated kinesin lacking much of the stalk region. Here we have measured close-to-full-length kinesin (K888) in the presence of low concentrations (400-800 nM) of ATP. We have used the technique of two-dimensional SHREC (Single molecule High-REsolution Co-localization), a method that can simultaneously monitor the position of two quantum dots on the kinesin with nanometer resolution; one quantum dot is on the motor domain and another is at one of several positions near the cargo-binding domain. Our results indicate that unlike the neck coiled-coil, the rest of the stalk does not continue in the tangent-plane, but rather directs the cargo to be above the motor-domains in the radial direction. In addition, by examining the on-axis position of motile kinesin under 400 nM ATP, we observe that the stalk occasionally translocated the cargo from the front to the back of the motor domain or vice versa when one of the motor domains dissociates from the microtubule. This suggests that both of the motor domains are bound to the microtubule during the ATP waiting state.

5.2 INTRODUCTION AND BACKGROUND

Kinesin-1, also called conventional kinesin, "walks" with its motor domains in a hand-over-hand fashion, taking 8 nm center-of-mass steps and 16 nm step-sizes[1–3]. Inside the crowded environment of the cell, kinesin must avoid bumping into molecules so it can move processively for several microns at high velocity towards the plus-end of microtubules. It does this with cargo ranging in size from a few nanometers to several microns. To understand how cargoes can be transported without significant steric hindrance, it is important to understand the cargo placement relative to the microtubule (Fig. 5.1).

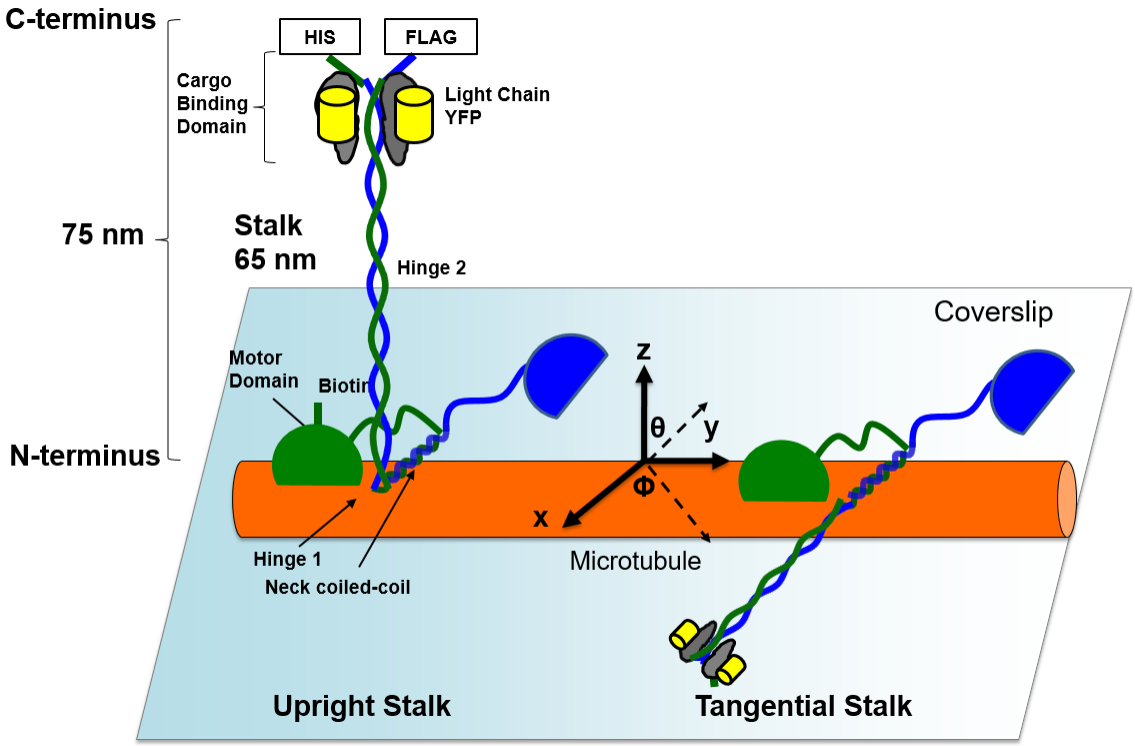

Figure 5.1. Diagram of Kinesin 888 construct used in the study.

Kinesin has a contour length of roughly 75 nm. The microtubule is in the x-y plane, which is also the plane of imaging. We define the direction that kinesin travels toward as the on-axis direction (x-axis). The y-axis is the direction tangential to the microtubule (in the optic plane) while the z-axis is perpendicular to the plane that the

microtubules lie on. Kinesin's neck coiled-coil lies horizontally against the microtubule up to Hinge 1. The question is in what direction does the remainder of the stalk go in, in particular, continue along the (x-) y-direction or take a turn and head in the z-direction? Here it is shown along the z-direction.

The position of the cargo is determined by the connection of the cargo to the kinesin, that consists of a cargo-binding domain (CBD), which is at the end of a long, ~65 nm, α-helical coiled-coil that is relatively rigid except for two flexible hinge regions, followed by a neck coiled-coil region ending in the motor domains (Fig. 5.1)[4,5]. The flexible hinges, as well as the neck coiled-coil region at the beginning of the stalk, govern the position of the stalk with regards to the motor domain and the microtubule. Hinge 2, (about half-way up the stalk) is known to be flexible, bending over to cause the stalk to interact with the motor domain in the absence of cargo, and remaining relatively straight with bound cargo[6,7]. The exact function of Hinge 1 (immediately after the motor-domain), is not known, but without it, kinesin motility is severely impaired[8].

The preponderance of evidence suggests that the neck coiled-coil tends to lie close to the microtubule, at least in kinesin mutants. Cryoelectron microcopy on the kinesin-tubulin complex indirectly supports this claim[9]. Thorn et al., studied K560 without Hinge 2, and showed increasing positive charges in the neck coiled-coil region improved run length by as much as 4-fold. Presumably, this arises from charge-charge interaction between the neck coiled-coil and the tubulin, implying a close interaction[10]. Martin et al. tested K401 without ATP, which contained the neck coiled-coil but was missing Hinge 1 and beyond. They used Fluorescence Resonance Energy Transfer (FRET) measurements which indicated that the end of the neck coiled-coil region lies only $4 \pm 5°$ up from the tangent plane[11]. The authors could not experimentally distinguish between the neck coiled-coil being aligned with the microtubule direction (called the axial direction, or $(r,\theta,\Phi = y, 90^{\circ}, 90^{\circ}$, Fig. 5.1) or being perpendicular to this direction in the tangent

plane (r,θ,Φ = x ,90˚, 0˚) Nevertheless, they argued that the stalk must be at r,θ,Φ = x ,90˚, 0˚ due to structural constraints, namely that the stalk would not interfere with walking of the motor domains. Finally, Schaap et al. did AFM studies on K433 and showed images of kinesin where the stalk came out r,θ,Φ = x ,90˚, 0˚ [12]. The experiment was also done using truncated kinesin lacking much of the stalk.

We wish to understand, in the presence of ATP, whether the stalk of kinesin after Hinge 1 continues along the direction tangential to the microtubule surface (Fig. 5.1, right-hand side: r,θ,Φ = x ,90˚, 0˚) or takes a roughly right-handed turn to move the cargo away from the tangential direction of the microtubule (Fig. 5.1, left-hand side, r,θ,Φ = z ,0˚, 0˚). Fig. 1 shows a schematic where the kinesin is positioned on top of the microtubule, such that the axis of incoming light (z-axis) is parallel to the radial direction of the microtubule. With kinesin binding to the top of the microtubule, if the stalk lies in the radial direction with respect to the microtubule (r,θ,Φ = z ,0˚, 0˚) , it will result in a minimum 2D distance in the x-y plane, which is the plane that is parallel to the polarization of the incoming light. On the other hand, if the stalk extends in the tangential direction (r,θ,Φ = x ,90˚, 0˚) it will result in a maximum 2D distance. Although the kinesin may bind in all directions around the microtubule, the distribution of the difference in the x-axis (off-axis direction) can be used to estimate the accessible microtubule surface that is available for the kinesins to bind to.

To determine the position of both the cargo and motor domains in the presence of an almost complete stalk, we used a nearly full-length kinesin (K888), which lacks the final 75 amino acids that are necessary for auto-inhibition[7]. To resolve the distance between the cargo and the motor domain, single molecule high-resolution co-localization (SHREC) was applied, which is a microscopy technique for localizing two-differently colored fluorophores, with approximately 10

nm resolution[13]. Using SHREC, we measured the two-dimensional distance, parallel to the coverslip, between two quantum dots. The quantum dot near the C-terminus was attached via variable linker lengths. Our results indicate that the cargo is not being carried tangential to the microtubule. This strongly implies that a significant bend must exist after the tangentially-oriented neck coiled-coil. In addition, monitoring both the CBD and motor domain position with nanometer precision and hundred millisecond temporal resolution reveals dynamic events, such as the occasional front-and-back translocation of the cargo with respect to the motor domain as kinesin is actively moving under low ATP condition (400 nM). From this we conclude that the dissociation of the rear motor-domain happens simultaneously with the cargo swinging either forward or backward. Our results clarify that during the "ATP-waiting state", both motor domains are bound to the microtubule.

5.3 RESULTS

A heterodimeric kinesin construct lacking the last 75 amino acids in the heavy chain (K888) was expressed using the baculovirus/insect cell expression system. One heavy chain contained a C-terminal His-tag and a biotin at the N-terminus, and the other heavy chain contained only a C-terminal FLAG-tag. The heavy chain was co-expressed with a kinesin light chain with a C-terminal YFP tag. The kinesin was simultaneously labeled with two differently colored quantum dots, one near its cargo binding domain (CBD), and the other at the N-terminus of the motor domain (Fig. 5.1). The biotinylated N-terminus of one of the two heavy chains of the heterodimer was labeled with a streptavidin conjugated quantum dot (Qdot-SA). For the Qdot labeling near the CBD, one of three alternative strategies was used. First, to label the His-tagged heavy chain, a Qdot was bound via two antibodies, namely an anti-HIS antibody followed by a

Qdot conjugated to goat anti-mouse antibody. Second, the Flag-tagged heavy chain was labeled using a Qdot conjugated to anti-FLAG antibody. Lastly, a nanobody specific to GFP/YFP was used to label the light chain (Fig. 5.1). (The nanobody is a 14 kDa antibody from llama, specific to a GFP/YFP, known as GFP-binding Protein, or GBP[14].) The lengths of antibody-linkers are estimated to be 20, 10, and 4 nm, respectively.

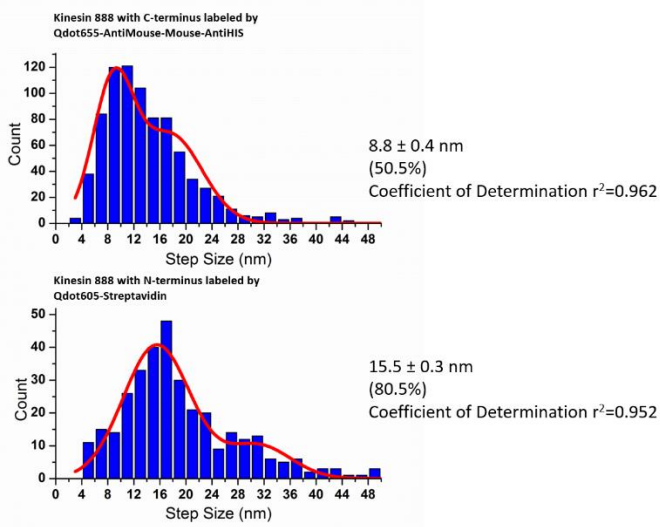

Figure 5.2. Step Size Histograms of Kinesin Labeled at CBD and Motor Domain. Kinesin motility trace was collected at 400nM ATP, and the trace was fitted using a step size finding algorithm. The resulting step sizes were collected and histograms were compiled (step size >50nm were omitted, which accounts for 0.8% of the cargo and 6.4% of the motor domain steps). The step size histograms were fitted to 2 gaussians with centers located at x and 2x. Kinesin labeled at the c-terminus takes predominantly 8.8±0.4 nm step (50.5%, N=24, center±SE) with undetected step resulting in an 8.8x2nm double step. In contrast, the kinesin labeled at the motor domain takes a 15.5± 0.3 nm step (80.5%, N=20, center±SE). These step sizes are what one would expect if the kinesin was properly labeled at cargo binding domain and motor domain.

To ensure that the Qdots were attached to the correct locations on the kinesin (i.e. the C- or the N-termini), the kinesin step-size was measured when only one location was labeled. We

found that the step size of kinesin labeled at the C-terminal HIS-tag or the N-terminal biotin tag showed the expected step sizes of 8.8 ± 0.4 nm and 15.5 ± 0.3 nm, respectively (Fig. 5.2.). Controls to make sure that the Qdots do not label kinesins non-specifically during the dual labeling process were also conducted.

To test the accuracy of how well we correct for chromatic aberration between the two channels using a mapping function generated from a set of nanoholes, we used our previous technique to measure the end-to-end distance of two organic dyes, Cy3 and Atto633N, attached to DNA molecules that are 51 and 68 base pairs apart[15]. We obtained distances of 15.4 nm and 22 nm (Fig. 5.3.). Our result agrees with the expected distance (17.3 nm and 23.0 nm) between the dyes within registration error (4 nm), and the distance difference between the two DNAs, confirming the accuracy of our method.

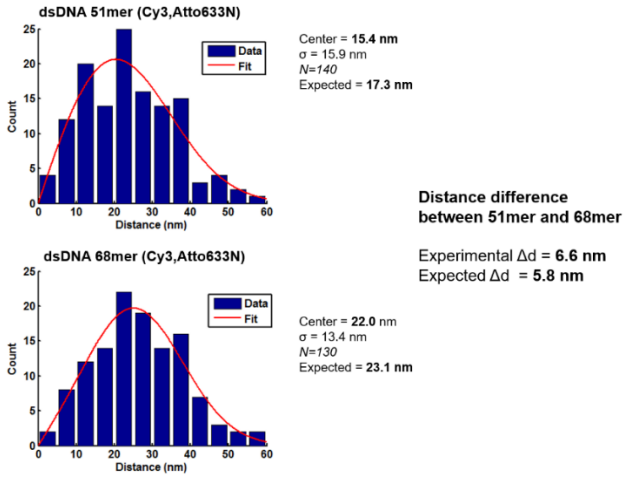

Figure 5.3. End-to-End distance Determining of 51mer and 68mer DNA Using SHREC. Histograms of the end-to-end distance of DNA 51mer and 68mer were compiled and fitted to specialized gaussian function. The center for the 51mer DNA is determined to be 15.4nm, where the expected distance is 17.3nm as approximately by a rigid rod. The center for the 68mer DNA was 22.0nm. Both experimentally measured distance were smaller than the expected distance by 1-2 nm. However, the difference between the two distance is accurate to within 1 nm. Given that the typical registration error of co-localization is 4nm, and the localization accuracy of each dye is 7-9nm the average distance determined

from the center and their difference is accurate. This gives up confidence that our SHREC method will be accurate when applied to Qdots which are more photostable, and for determining a larger difference between conformations (0 to 75 nm).

As kinesin actively walks on the microtubule in the presence of ATP, the relative position between the CBD and the motor domain Qdots can be decomposed in terms of the on- and off-axis of the microtubule (Fig. 5.4A). The on-axis (called the y-axis) offset is parallel to the direction that kinesin is walking towards, and the off-axis offset (called the x-axis) is the direction that is tangential to the microtubule and parallel to the coverslip. Separating the two axes allow us to examine whether the kinesin carries its cargo with any preference for a particular direction. An example trace, Fig. 5.4B, is obtained from a kinesin labeled with a Qdot attached to the CBD via 2 antibodies (green) and to the N-terminal biotin with Qdot-SA (red). The distance between the two Qdots, for both the on- and off-axes, are shown immediately below in Fig. 5.4B. A 2D histogram of the on-axis (y-axis) difference between the motor-domain Qdot and the CBD Qdot and the off-axis (x-axis) difference, correlated in time, is shown in Fig. 5.4C. The histogram is a two-dimensional projection of the position of the cargo using the motor domain as the reference point at (0,0). That there is a single peak at about (0,0) indicates that the cargo is primarily sitting above the motor domain: if the stalk was tangential, the most probable position would be far from zero in the off-axis direction. Furthermore, the cargo also has a wider distribution along the front and back direction (σ_y = 31.5 nm) than the left-right direction (σ_x = 20.7 nm). The implication is that the cargo can be positioned in a greater range of angles along the direction of motion rather than perpendicular to it.

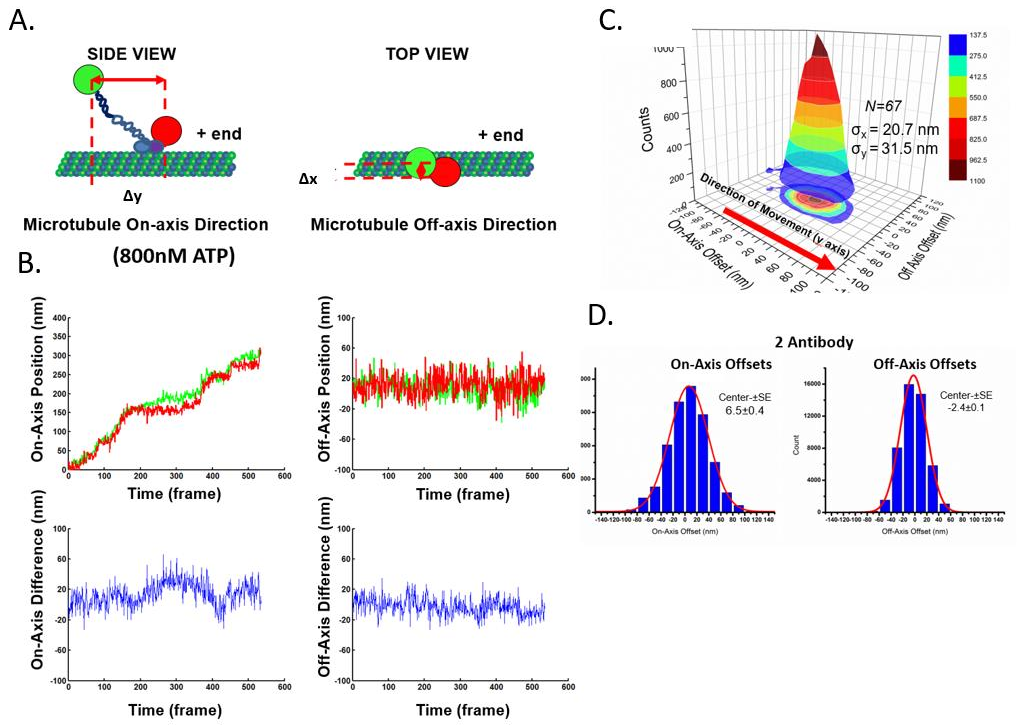

Figure 5.4. Analysis of on and off-microtubule axis offset. A) Illustration of kinesin orientation in terms of on and off microtubule axis. Here the on-axis direction is the y-axis, and off-axis direction is the x-axis. B) Example of on and off axis kinesin motility traces from Qdots attached to cargo binding domain via 2 antibodies (green) and motor domain via a SA-Qdot (red). The on and off axis differences are calculated by subtracting the position of red trace from the green trace. C) 2D histogram that depicts the most probable position of kinesin's cargo in reference to the motor domain. The CBD of kinesin was labeled with Qdot-anti Mouse conjugated to Mouse-anti HIS, and motor domain was labeled using a streptavidin Qdot. The position of the cargo is color coded in the histogram based on the number of times a particular offset is observed using a 20 nm bin size in both direction. The most probable position for the cargo is clearly centered around the motor domain at (0,0). The distribution is wider in the on-axis direction (y-axis) than off-axis (x-axis) direction, is likely caused by the translocation of cargo front and back of the motor domain within a trace. C) The difference between the Qdots attached to tail and head of kinesin in the on-axis direction (Δy) and off-axis direction (Δx) depending on the attachment method: 2 Antibodyis calculated from each frame of the kinesin motility movie, and the difference in on and off axis distance were compiled into a histogram. The results obtained using other antibody labeling methods are summarized in Table 1.

Next, we fit the off-axis and the on-axis positions of the cargo separately to a Gaussian distribution to see if the cargo has a preference between the left-and-right, or between the front- and back of the motor domain (Fig. 5.4D). We found that the on-axis and off-axis center was at 6.5 ± 0.4 nm, and -2.4 ± 0.1 nm, respectively, or close to zero. This implies little preference. Furthermore its range is fairly limited: from +/- 60 nm, and never less than -40 nm or greater than +30 nm, when we eliminate the effect of noise in the off-axis data by averaging. Combining the observation that the center of the distribution for the off-axis offset is about zero with a limited range, implies that unlike the neck coiled-coil, the stalk of kinesin is not tangential to the microtubule; otherwise the center of the distribution of the off-axis difference would be biased significantly towards the negative direction.

Previously we have stated that the stalk of kinesin is not tangential to the microtubule. What exactly then is the conformations of the kinesin's stalk? In order for the cargo to be directly above the motor domain, there has to be a bent at either hinge I or II after the tangentially oriented neck-coiled coil. If hinge II is bent in the wild type, removing hinge II would straighten the kinesin, causing a larger height to be measured.

To measure the height of kinesin, we can examine the spread of off-axis offsets, because these extrema would be the height of the kinesin when it binds to the side of the microtubule. A larger off-axis offset to be measured when kinesin binds to the side of the microtubule. In the hinge II deleted mutant, we did not observe an increase in the range of maximum and minimum off-axis offset (Table 1).

	Off-axis offset	FWHM	On-axis offset	FWHM	Off-Axis
2 AB	-2.4±0.1	52.3	6.5±0.4	76.3	30/-40
1 AB	-2.7±0.5	60.6	0.6±0.6	68.0	40/-60
GBP	1.2±0.5	52.8	0.0±0.3	64.6	50/-40
1 AB Organic Dye	0.5±0.6	48.8	2.9±0.4	56.4	50/-60
2 AB ΔH2	1.5±1.1	61.0	4.1±0.5	67.9	40/-40
2 AB MTΔC	-4.2±0.3	56.5	5.0±1.6	83.2	40/-50

Table 5.1. Head to Tail Distance of Kinesin-1 Measured From Various Constructs and Probes

The range of off-axis offset is 30 to -40 nm in the wild type, and 40 to -40 nm in the hinge II deleted mutant, implying that kinesin was already fully stretched to begin with in our measurement of wild type. Another possibility is that the kinesin remains folded even with hinge II removed. The second scenario is less likely, since the alpha coiled-coils are not really flexible elements that can keep the kinesin folded at all times.

The question is whether a distance of 40 to -40 nm makes sense as the height of the kinesin when binding to the side of the microtubule, or is the kinesin being surface restricted somehow limited the kinesin from binding to the side. To avoid steric restriction on kinesin carrying a cargo so that it can bind to the side of microtubules, the same experiments were performed on axoneme and microtubule suspended on 440 nm beads, and we've obtained more or less the same result (Data not shown). We expected to see some kinesins binding to the side of the microtubule in these experimental settings. In our results, we observed the spread of distribution widen from 30 to -40 nm to 50 to -50 nm, it never quite reach the full contour length of kinesin. This can be explained by the size of the probes, since one of the Qdots is attached to

the N-terminus of motor domain, we would expect the center of the Qdot to sit ~10 nm above the motor domain, shrinking the possible distance that can be measured from the tail domain to the motor domain. As we decrease the size of the probes, from Qdots to organic dyes, our distribution of off-axis distance increases up to 50 to-60 nm which is close to the length of kinesin from hinge I and above. Therefore, using surface bound microtubule and the massive size of Qd did somehow restrict us from measuring the complete ~60 nm contour length. Although a larger off-axis should be observed when using 2 antibodies instead one antibody or a small nanobody, we argue that it's not certain how these antibody may contribute to the height of the kinesin. For instance, we did however observed an increase in the width of the on-axis distribution, implying that the antibodies adding to the distance in the on-axis direction, or the front and back of the kinesin, and not directly to the top of kinesin.

Since Hinge II does not play a role in changing the height of kinesin, we conclude that the Hinge II is not normally folded for kinesin in motion. The bent that redirects the cargo to above the motor domain from a tangentially oriented neck-coiled coil occurs at Hinge I of the kinesin.

The C-terminus of the (α and β) tubulin heterodimer is hypothesized to interact with the neck coiled-coil region. Originally, this was hypothesized to cause the stalk to become tangential to the microtubule with a bias to one side[10]. Subsequent experiments using a truncated K401 construct found this was not the case; the neck coiled-coil orients tangential to the microtubule even with C-terminus of the tubulin cleaved[11]. We wanted to see whether the same was true using our nearly full-length (K888) kinesin. The C-terminus of tubulin was therefore removed by subtilisin digestion[16]. Experiments were conducted to make sure the subtilisin digestion was complete (Fig. 5.5.AB). We found that the center of the distribution in the off-axis direction only

shifted slightly from -2.4 nm to -4.2 nm (Table 1). This difference is smaller than the registration error of the two-color experiment (4 nm), i.e. is not significant. Our result therefore confirms the previous work by Martin et al. where they discovered no change in *neck coiled-coil* orientation after removal of the C-terminus from tubulin. We conclude that there is no significant effect on the overall direction of the *stalk* when the tubulin C-terminus was removed.

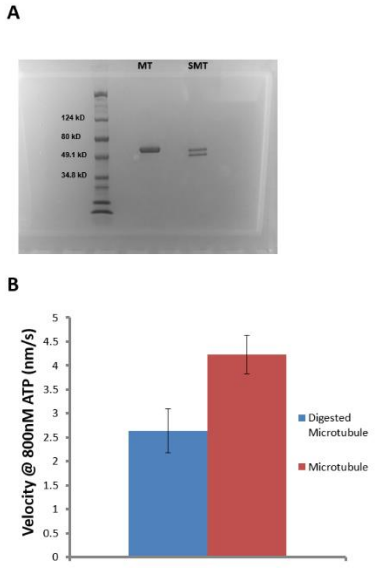

Figure 5.5. SDS-Gel Electrophoresis of Microtubule and Digested Microtubule. After digestion with subtilisin, a SDS-PAGE was performed to verify the completion of digestion activity. Comparing the normal microtubule (MT), and digested microtubule (SMT), the digested microtubule shows 2 bands with less molecular weight which are typically observed after subtilisin digestion. B) Velocity assay performed on kinesin on subtilisin digested microtubule and normal microtubule. The velocity of kinesin on digested microtubule was 2.64±0.45nm/s (n=23), whereas on normal microtubule under the same ATP concentration, the velocity of kinesin was 4.23±0.4nm/s (n=19).

By lowering the ATP concentration from 800 nM to 400 nM, individual steps were discernable. We observed the CBD and motor domain alternating the leading/rear position in the on-axis direction, i.e. the cargo (green) of kinesin abruptly switches from the front of the motor

domain (red) to the back of the motor domain and vice versa (Fig. 5.6.). Statistically, we observed the switch occurred 8.6% (54 switching event observed over 626 steps) of the total number of steps taken.

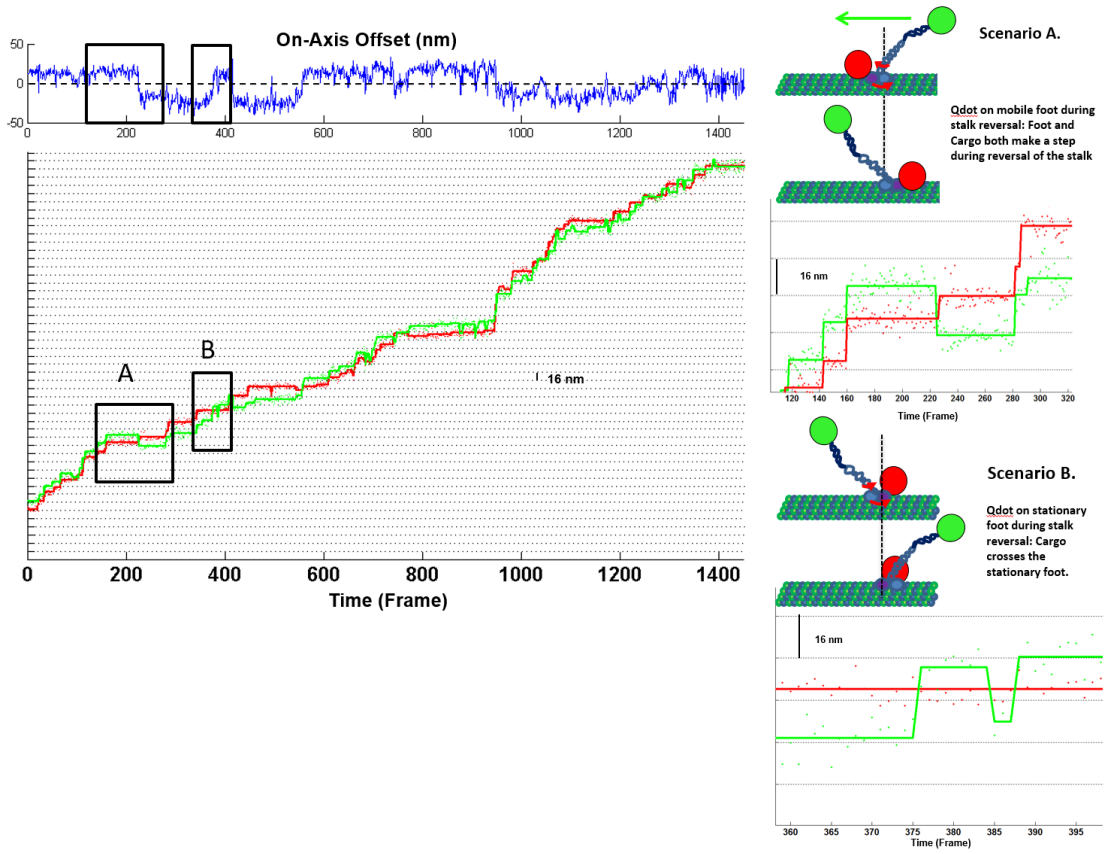

Figure 5.6. Dynamics between Cargo and Motor Domain at 400 nM ATP Concentration. An example trace is shown where the Cargo (Green) and Motor Domain (Red) of kinesin are both monitored as kinesin is actively walking along the on-axis direction. The solid lines are fitted results from step finding algorithm. At times the cargo and motor domain switches in role in terms of which domain is in front of one another. The majority of the switches can be categorized in two proposed scenarios. Scenario A happens when both the cargo (green circle) and the labeled motor domain (red circle) step together in order to switch the leading position. Scenario B occurs when the lead position change due to cargo crossing a labeled stationary motor domain, while the unlabeled motor domain takes a step.

There are two ways for the cargo and motor domains to move with respect to each other that would cause such a switch (Fig. 5.6). The Qdot on the motor domain is either bound to the foot which takes a step, i.e. the rear foot stepping forward (Scenario A), or is bound to the stationary motor domain (Scenario B). In either case, the cargo and motor domain change lead as a result of cargo movement. Scenario A results in the simultaneous movement of both cargo and motor domain in the trace. We observed this to happen 43% of the time (23 out of 54 total switching events). In scenario B, the cargo appears to cross the stationary Qdot on the motor domain in the trace. This occurs 41% (22 out of 54 switching event) of the total events observed. In the remaining 16% of the time (9 out of 54 switching event), the kinesin appears to take a step (i.e., the motor domain moves), but the cargo appears not to move. We believe this is because of the presence of noise in our measurement, or due to something interfering with the cargo moving. We also measured steps sizes of these dual-labeled kinesins to make sure that the Qdots are labeled at the proper positions (Fig. 5.7.) and that the 16 nm steps are "real", i.e. not simply a matter of missing two 8 nm steps.

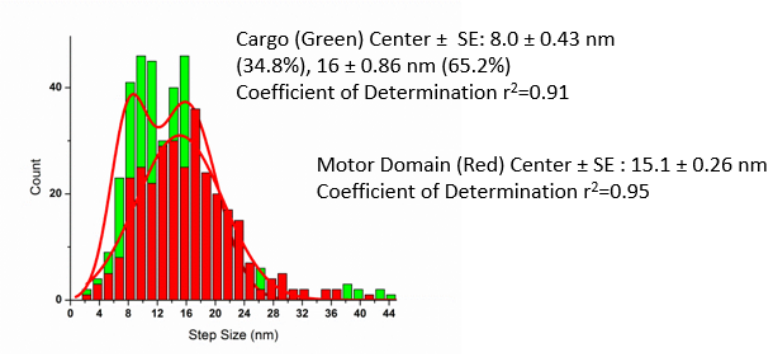

Figure 5.7. A step size histogram is compiled from a total of 9 traces where abrupt switching was observed at 400 nM ATP (Green, N=396 steps, Red, N=313 steps). Step size greater than 45nm are omitted in the plot which accounts for less than 1% of the total number of steps for both motors. The cargo Qdot is shown to take predominantly 8.0 ± 0.43 nm (center± SE) and steps that are twice of the magnitude, whereas the motor domain takes predominantly 15.1 ± 0.26 nm steps (center± SE).

5.3 DISCUSSION

Through the use of SHREC we have successfully monitored the position of both the CBD and the motor domain as kinesin walks along the microtubule. The advantage of the SHREC method is that the conformation of the stalk is based on direct observation of the CBD and motor domain position, and therefore the data interpretation is straightforward. We separately looked at the off-axis motion and the on-axis motion with respect to the microtubule direction. The off-axis motion leads us to conclude that the cargo is upright. However, the on-axis motion indicates that while the average position is close to having the cargo above the motor domain, there is a wide variance. At an ATP concentration where single steps can be resolved, we find that the cargo is sometimes thrown forward, and sometime thrown backwards, with respect to the motor domain. This has important implications for what the "ATP-waiting state" looks like. For both the on- and off-axis directions, the presence or absence of the C-terminus of tubulin does not affect the results.

Is the cargo upright or tangential to the microtubule? Two previous studies have looked at the direction of the stalk[12,17]. The first study, by Kerssemakers et al., measured the distance between the CBD and motor domain of full-length kinesin along the z-direction, where the microtubule is in the x-y plane. They did this by preferentially exciting the microtubule as a function of z through an interferometric technique. They found the contour length of kinesin to be only 17 nm in the z-direction, as opposed to the full height of kinesin (~75 nm). The authors concluded that the stalk of kinesin is either compressed, or is laid down flat and tangential to the microtubule.

Our results show that the stalk is not tangential to the microtubule, since both the on- and off-axis difference is centered at zero, implying that the cargo is most frequently found above the

motor domain. That leaves the compressed stalk model the consensus model between our study and that of Kerssmakers et al., although the differences between a gliding assay, used by Kerssemakers et al., and our motility assay, prevent a definitive conclusion. While a compressed stalk would also lead to a comparatively smaller 2D distance between motor-domain and cargo, our results were obtained with a small cargo (~20 nm diameter of the quantum dot), which would fully activate the kinesin while exhibit significantly lower forces of compression than in the gliding assay by Kerssemakers et al.

The second study used AFM measurement of the kinesins placed on the microtubule[12]. This study shows that the stalk is oriented tangential to the microtubule, just like the neck coiled-coil region. However, the construct used was a truncated kinesin mutant (K433), which lacks most of the stalk region above Hinge I. Also, the experiment was conducted in the presence of AMP-PNP (a non-hydrolyzable analogue of ATP), such that the kinesins were not motile during the measurement.

Our results, obtained while kinesin walks along the microtubule, indicate that the cargo carried by a nearly full-length kinesin is directly above the motor domain of kinesin. Its disposition is insensitive to the presence of hinge II and the C-terminus of tubulin. Based on published findings that the neck coiled-coil region is tangential to the microtubule, this implies that a 90° turn must occur somewhere after the neck coiled-coil region. That is, the stalk must be bent at Hinge I with the remainder of the kinesin stalk being rigid, such that the cargo is above the microtubule in the z-dimension. Hinge I is the only element that is capable of bending and directing the cargo above the motor domain to avoid steric clashes with other proteins on the microtubule. Therefore, the most efficient way for kinesin to carry the cargo would be to extend its cargo and stalk in the out-of-plane (z-) direction.

At lower ATP concentration (400 nM), where single step-sizes are discernable, we observed the cargo suddenly change its on-axis position, from the front to the back of the motor-domain or vice versa (Fig 5.6). This appears to be a two-state transition (Top). One possibility is that this translation of the cargo involves a twisting of the stalk. This was actually observed in an optical trapping experiment: An asymmetric bead was put on the cargo and the direction of the asymmetry flipped 180° every 2% of the steps (depending on ATP concentration) [11]. Based on the rarity of the switching event during motility in our result (8.6%) and the change in the position of the cargo being two-state (front and back), we believe that we are observing the same phenomenon, namely an occasional 180° rotation of the stalk.

When using low concentration of ATP (400 nM), the kinesin is in the ATP-waiting-state the majority of the time. This state has either one motor domain bound to the microtubule, or both motor domains bound. For the two-motor-domain bound case, we would see the cargo change direction (i.e. front-to-back or back-to-front) *simultaneously* with the stepping of the motor domain. In fact, we do see this happening 43% of the time, slightly less than the 50% predicted for the two-head model. The other 50% occurs when the label is bound to the stationary head; In-fact, we see this happens 41%. In the remaining 16%, the cargo doesn't move, even when the motor domain takes a step, a clearly unnatural configuration. On the other hand, if only one motor domain is bound during the ATP-waiting-state, the stalk would rotate freely during the ATP-waiting state and rarely coincide with the stepping of the motor domain. The fact that the cargo changes direction with (43%) and without (41%) the stepping of the labeled motor domain with roughly equal frequency, clearly shows that this is not the case.

5.4 CONCLUSION

By measuring both the end-to-end (on-axis) distance and the off-axis distance of an almost full-length kinesin while it walks using the method of two-dimensional SHREC. We have determined that the stalk of kinesin is bent at hinge I unlike the tangentially oriented neck coiled-coil. At low ATP concentration where kinesin spends the majority of the mechanochemical cycle waiting for ATP, we found that the cargo suddenly changes direction between the front and the back of the motor domain most frequently when one of the motor domains take a step. This implies that when kinesin is waiting for ATP, both motor domains remain bound to the microtubule, preventing the stalk from changing direction.

5.5 METHODS

Preparation of Kinesin Constructs Kinesin constructs used in this work, (K888, K888ΔH2) expression and purification are prepared by Kathy Trybus Lab in U of Vermont.

Microtubule and Surface Preparation Tubulin, biotin tubulin, and tubulin conjugated to Hilyte 488 were mixed in ratio of 25:3.13:1 at a total concentration of 5.8mg/mL and polymerized in polymerizing buffer that consists of 3mM GTP, 35% glycerol and BRB80 buffer (80mM PIPES pH6.8, 1mM EGTA, 1mM $MgCl_2$) at 37 degree C for 30 minutes. The sample was then diluted 7 times in taxol GTP buffer consists of BRB80, 1mM GTP, and 20μM paclitaxel. The diluted microtubules were then centrifuged at 15,000×g for 30 minutes at room temperature. Supernatant was discarded, and the microtubule pellet was resuspended in taxol GTP buffer at a final concentration of 0.58mg/mL. Microtubules were then immobilized on the surface of the coverslip for experiment. Sample chambers were made from a 5% biotin-PEG slide, and 0.5mg/mL of neutravidin was added and incubated for 5 minutes. Excess and unbound neutravidin were washed

away by Motility buffer and BSA (8mg/mL BSA in MB, see main text). Microtubules were then diluted 10X in taxol buffer consist of MB-BSA, 20 μM paclitaxel, and incubated for 5 minutes in the neutravidin coated chamber. To remove unbound microtubule and block free neutravidin binding site in the chamber, 0.1mM biotin were added to the taxol buffer and flown through the chamber.

Quantum Dots Conjugation and Labeling the Kinesin Quantum dots conjugated to 2 antibodies were generated by using Quantum dot 655 anti-Mouse (Life Technologies), incubated with Mouse anti-HIS antibody for 30 minutes in motility buffer (30mM HEPES pH 7.2, 50mM KAcetate, 2mM Mg-Acetate, 1mM EGTA, 8mg/mL BSA), 1mM THP, and 1.6 uM ATP. Quantum dots conjugated to anti-FLAG antibody was generated by using the Invitrogen Quantum dot conjugation kit (Life Technologies). Quantum dots conjugated to GFP binding nanobody was custom made and has been previously published [Ref Yong Paper]. Conjugated GBP-Qdot was tested on kinesin (K888) lacking the YFP to ensure there was no non-specific binding to the kinesin. The Quantum dots used to label the cargo binding domain were incubated with kinesin diluted in dilution buffer that consists of motility buffer, 1 mM THP and 1.6 uM ATP at 6:1 Quantum dot to kinesin ratio for 30 minutes. To avoid having multiple kinesins bound to the same Qdots, the molar ratio between Qdots and kinesin was at least 6:1. In this way, there are many times more Qdots than kinesin and only 1% of the Qdots will have more than 1 kinesin bound according to Poisson statistic. Quantum dot 605 Streptavidin conjugate (Life Technologies) were blocked to prevent non-specific binding by diluting it 2 fold with SuperBlock Buffer (Thermo Scientific) for 15 minutes. The blocked SA-Qd605 were then added to CBD labeled kinesin at 7:1 ratio and incubated for 30 minutes on ice. At the end of the 30 minutes, 0.9 mM of biotin was added to the kinesin quantum dots mixture to saturate the free

streptavidin binding sites on the Qdot-SA. The percent of kinesin labeled with both Qdots (specific to CBD and motor domain) that showed motility under the influence of ATP was roughly 15-35% of the total moving Qdots observed in the CBD Qdot channel. The experiments are performed within 3 hours after saturation with biotin to avoid nonspecific binding of Qdots to kinesin due to prolonged incubation.

Motility Assay and Imaging Setup Imaging was performed on sample chambers constructed by attaching 5% PEG-Biotin coverslip to channels created by gaps between the double-sided tapes. Motility assay was performed using motility buffer, 2mM THP (reducing agent), 0.02mM biotin, 20μM paclitaxel (microtubule stabilizing agent), 50nM protocatechuate-3,4-dioxygenas (PCD), protocatechuic acid (1mg/mL), and a final ATP concentration of 400-800 nM. Images were collected at 150ms exposure time. The quantum dot labeled at C and N terminus were both excited with 488 nm argon-ion laser (Melles Griot) in TIR using an inverted microscope (Olympus). The emission passes through a divider (Optosplit II, Cairn Research) based on wavelengths, causing the fluorescence image to occupy two halves of the CCD camera (Andor). Bandpass filter 655/15 was used for the Qdot655 emission channel, and either a 605/15 or 593/43 filter was used for the Qdot605 channel.

Calibration with Nanoholes and Data Analysis To co-localize the two emission channels, a mapping function was generated from images of a slide full of diffraction limited holes that are 1.5 um apart imaged in brightfield. Mapping function was created from the brightfield image using previously published algorithm written in matlab[18]. Kinesin motility traces were processed and analyzed with custom matlab script. Basically, images containing motile quantum dots that are co-localized in both channels were cropped. The point-spread function of the quantum dot fluorescence from both channels was fitted to a 2D Gaussian in order to determine the center

position. Center position in x and y were obtained per frame, and traces were screened for outliers caused by blinking of the quantum dots and quantum dots that diffused into the field of view. Over a short distance that the kinesin traveled under 400-800 nM ATP concentration the distance traveled is relatively straight which allow us to rotate the trace linearly so that the direction of movement is only in the x-axis. To determine step sizes, the position trace in x-axis after rotation was inputted into step finder algorithm[19]. The on and off axis offsets are calculated by subtracting the rotated x and y position of the motor domain from the x and y position of the cargo for each frame of the movie. Distance between two Qdots is obtained by distance formula using position of cargo and motor domain Qdot per frame. An average distance is calculated per kinesin trace. The average distances from each trace are then used to compile a histogram. The histogram is fitted using a specialized Gaussian function suitable for determining the expected value of a broad distribution obtained from measuring 2D distance[20].

5.6 REFERENCE

1. Svoboda, K., Schmidt, C. F., Schnapp, B. J. & Block, S. M. Direct observation of kinesin stepping by optical trapping interferometry. *Nature* **365,** 721–727 (1993).
2. Yildiz, A., Tomishige, M., Vale, R. D. & Selvin, P. R. Kinesin Walks Hand-Over-Hand. *Science* **303,** 676–678 (2004).
3. Asbury, C. L., Fehr, A. N. & Block, S. M. Kinesin Moves by an Asymmetric Hand-Over-Hand Mechanism. *Science* **302,** 2130–2134 (2003).
4. Scholey, J. M., Heuser, J., Yang, J. T. & Goldstein, L. S. B. Identification of globular mechanochemical heads of kinesin. *Nature* **338,** 355–357 (1989).

5. de Cuevas, M., Tao, T. & Goldstein, L. S. Evidence that the stalk of Drosophila kinesin heavy chain is an alpha-helical coiled coil. *J. Cell Biol.* **116,** 957–965 (1992).
6. Dietrich, K. A. *et al.* The kinesin-1 motor protein is regulated by a direct interaction of its head and tail. *Proc. Natl. Acad. Sci.* **105,** 8938–8943 (2008).
7. Lu, H., Ali, M. Y., Bookwalter, C. S., Warshaw, D. M. & Trybus, K. M. Diffusive movement of processive kinesin-1 on microtubules. *Traffic Cph. Den.* **10,** 1429–1438 (2009).
8. Bathe, F. *et al.* The complex interplay between the neck and hinge domains in kinesin-1 dimerization and motor activity. *Mol. Biol. Cell* **16,** 3529–3537 (2005).
9. Skiniotis, G. *et al.* Nucleotide-induced conformations in the neck region of dimeric kinesin. *EMBO J.* **22,** 1518–1528 (2003).
10. Thorn, K. S., Ubersax, J. A. & Vale, R. D. Engineering the processive run length of the kinesin motor. *J. Cell Biol.* **151,** 1093–1100 (2000).
11. Martin, D. S., Fathi, R., Mitchison, T. J. & Gelles, J. FRET measurements of kinesin neck orientation reveal a structural basis for processivity and asymmetry. *Proc. Natl. Acad. Sci. U. S. A.* **107,** 5453–5458 (2010).
12. Schaap, I. A. T., Carrasco, C., de Pablo, P. J. & Schmidt, C. F. Kinesin walks the line: single motors observed by atomic force microscopy. *Biophys. J.* **100,** 2450–2456 (2011).
13. Churchman, L. S., Okten, Z., Rock, R. S., Dawson, J. F. & Spudich, J. A. Single molecule high-resolution colocalization of Cy3 and Cy5 attached to macromolecules measures intramolecular distances through time. *Proc. Natl. Acad. Sci. U. S. A.* **102,** 1419–1423 (2005).

14. Rothbauer, U. *et al.* Targeting and tracing antigens in live cells with fluorescent nanobodies. *Nat. Methods* **3,** 887–889 (2006).
15. Wang, Y. *et al.* Small Quantum Dots Conjugated to Nanobodies as Immunofluorescence Probes for Nanometric Microscopy. *Bioconjug. Chem.* **25,** 2205–2211 (2014).
16. The C-Terminus of Tubulin Increases Cytoplasmic Dynein and Kinesin Processivity. Available at: http://www.sciencedirect.com/science/article/pii/S0006349500767439. (Accessed: 6th June 2016)
17. Kerssemakers, J., Howard, J., Hess, H. & Diez, S. The distance that kinesin-1 holds its cargo from the microtubule surface measured by fluorescence interference contrast microscopy. *Proc. Natl. Acad. Sci. U. S. A.* **103,** 15812–15817 (2006).
18. Single-Molecule Techniques: A Laboratory Manual. Available at: http://www.cshlpress.com/default.tpl?action=full&--eqskudatarq=642. (Accessed: 6th June 2016)
19. Kalafut, B. & Visscher, K. An objective, model-independent method for detection of non-uniform steps in noisy signals. *Comput. Phys. Commun.* **179,** 716–723 (2008).
20. Stirling Churchman, L., Flyvbjerg, H. & Spudich, J. A. A Non-Gaussian Distribution Quantifies Distances Measured with Fluorescence Localization Techniques. *Biophys. J.* **90,** 668–671 (2006).